AN ABSTRACT OF THE THESIS OF

Elanchezhian Somasundaram for the degree of Master of Science in Nuclear Engineering presented on October 7, 2011.

Title: Benchmarked Simulation of Antineutrino Source Terms for Light Water Reactors during Normal Operation and Diversion Scenarios

Abstract approved:

_____

Todd S. Palmer

Detection of reactor antineutrinos for non-proliferation applications has been researched extensively across the globe and is considered as a potential technology to remotely monitor reactor operations without any intrusions to reactor components. Reactor antineutrino detection experiments have been conducted in the past and have proven successful in detecting the changes in antineutrino source terms due to power level changes and to the changes due to fuel depletion within the core. However, the detector technology is still in its primitive stage to be successfully deployed for non-proliferation purposes. Simulation of reactor antineutrino signatures is vital to verify the experimental measurements. They also provide an insight into detector configurations required to monitor different reactor types and potential fuel diversion scenarios. In this thesis, the simulation of antineutrino signatures of light water reactors (LWRs) using industry standard reactor simulation tools, CASMO-4 and SIMULATE-3, is studied. Three different LWR reactors have been modeled and

different diversion scenarios involving uranium di-oxide (UO_2) and mixed oxide (MOX) fuel have been simulated. The simulation results are also benchmarked with the antineutrino counts measured by the SONGS1 antineutrino detector that was used to monitor the operation of San Onofre Nuclear Generating Station (SONGS), unit 2, cycle-13 during the period 2004-2005. A three-dimensional simulation of the reactor cores has been performed for improved accuracy of the detector response. Further, full core simulation allows reactor modeling without detailed information about the power histories of individual fuel assemblies, which was the case in previous research.

Benchmarked Simulation of Antineutrino Source Terms for Light Water Reactors during Normal Operation and Diversion Scenarios

by

Elanchezhian Somasundaram

A THESIS

submitted to

Oregon State University

in partial fulfillment of
the requirements for the
degree of

Master of Science

Presented October 7, 2011
Commencement June 2012

Master of Science thesis of Elanchezhian Somasundaram presented on October 7, 2011.

APPROVED:

_____

Major Professor, representing Nuclear Engineering

_____

Head of the Department of Nuclear Engineering and Radiation Health Physics

_____

Dean of the Graduate School

I understand that my thesis will become part of the permanent collection of Oregon State University libraries. My signature below authorizes release of my thesis to any reader upon request.

_____

Elanchezhian Somasundaram, Author

ACKNOWLEDGEMENT

I would like to thank my advisor, Dr. Todd Palmer for having me in his research group and giving me the opportunity to work on this project as a research assistant. I would also like to thank him for his valuable guidance throughout my graduate studies.

I also would like to thank Dr. Alexey Soldatov for his guidance in using the simulation tools and for providing insight on different diversion scenarios that helped me a lot during the course of the project.

I would also like to thank my project mates, Andra Shaughnessy and Topher Mathews for their valuable support.

I would also like to thank the Nuclear Engineering and Radiation Health Physics Department for providing me with the necessary facilities to successfully complete this thesis and the National Nuclear Security Administration Office of Non-Proliferation Research and Development (NA-22) for funding this project.

I would also like to thank my family and friends for all of the support and encouragement throughout my studies.

TABLE OF CONTENTS

Page

TABLE OF CONTENTS (Continued)

Page

LIST OF FIGURES

LIST OF FIGURES (Continued)

Figure Page

LIST OF TABLES

LIST OF APPENDIX TABLES

Benchmarked Simulation of Antineutrino Source Terms for Light Water Reactors during Normal Operation and Diversion Scenarios

1 Introduction

One of the major issues faced by the International Atomic Energy Agency (IAEA) in implementing the Nonproliferation Treaty (NPT) is the monitoring of nuclear reactors for proliferation activities. With the number of reactors expected to multiply rapidly in the near future, especially in developing countries, it will be very important to independently confirm self-reported reactor operations and ensure the fuel is used only for its intended purpose. Currently the only way to verify the fuel inventory of a reactor is based on the operator log book and verification of the spent fuel pools. These methods can be easily forged, making it essential to have an independent system that can monitor reactors without interfering with the reactor operations. Antineutrino detectors have proven to be potential candidates for remote monitoring of reactors. They are capable of gathering real time information on the status of the core, detecting diversion activities (removal of fuel assemblies with high plutonium content for weapons use) within the conversion time (1-3 months as specified by IAEA), and are less intrusive and simpler from the perspective of both the reactor operator and the safeguards agency (Bernstein, Wang, Gratta, & West, 2002) .

Another important application of remote reactor monitoring systems is to provide support for nations in their weapons reduction commitments. For instance, The United States and Russia have agreed on a Scientific and Technical Cooperation in the management of plutonium that is withdrawn from their weapons programs. According to this agreement (“ July 1998 Agreement”), each country has pledged to dispose of no less than 34 metric tons (MT) of this weapons grade (WG) plutonium, in a parallel time

frame, at an average annual rate of 2 MT. One approach to accomplish this task is to utilize the weapons grade (WG) material as fuel for commercial and research reactors in both countries. This material can be fabricated as Mixed Oxide Fuel (MOX) and used in reactors along with the normal Uranium Dioxide (UO_2) fuel. MOX fuel can also be fabricated from reprocessed depleted fuel; this fuel is designated as reactor grade MOX (RG MOX) based on the plutonium isotopic composition. Because both WG and RG MOX can be used in power and research reactors, there is an additional need for a verification mechanism to ensure the declared type and amount of fuel is utilized in the reactor (Gehin, Carbajo, & Ellis, 2004).

Antineutrino detectors for reactor monitoring have been researched around the globe and the results have been promising. Antineutrinos are particles produced during the β^- decay of radioisotopes. A simple negative β decay reaction is shown below.

$$n \rightarrow p + \beta^- + \bar{\nu}$$

An unstable radioisotope may become stable by converting its excess neutron (n) into a proton while emitting a β^- particle and an antineutrino ($\bar{\nu}$). The energy released during the process is converted into the kinetic energy of the β^- particle and the antineutrino. Depending on the parent nucleus, the fraction of the energy carried by the β^- particle and the antineutrino varies. This leads to antineutrinos being emitted with a spectrum of energies, depending on the nature of the materials and reactions occurring within the reactor.

In a reactor, the major source of antineutrinos is from the radioactive decay of fission products. Fission products are produced during reactor operation when the fuel

material undergoes fission by neutrons. Depending on the type of fuel material that undergoes fission, different fission products are produced. Each of these fission products, in turn, decays to form stable nuclei by different mechanisms, negative beta decay being the most common among them. Since the number and energy spectrum of emitted antineutrinos depends on the parent fission product nucleus, the antineutrino spectrum from the reactor gives an estimate of the ongoing fission rate and the nature of the fuel material that is undergoing fission.

The major fissile isotopes in a light water reactor are ^{235}U, ^{238}U, ^{239}Pu and ^{241}Pu. An example thermal fission reaction of ^{235}U resulting in the release of fission products, neutrons and energy is shown in the following equation:

$$U^{235} + n \rightarrow U^{236} \rightarrow Ba^{144} + Kr^{89} + 3n + 177MeV\ .$$

The beta decay of fission products formed in the above reaction is shown below:

$$Ba^{144} \rightarrow La^{144} + \beta^- + \bar{\nu} \rightarrow Ce^{144} + \beta^- + \bar{\nu} \rightarrow Pr^{144} + \beta^- + \bar{\nu}$$

$$Kr^{89} \rightarrow Rb^{89} + \beta^- + \bar{\nu} \rightarrow Sr^{89} + \beta^- + \bar{\nu} \rightarrow Y^{89} + \beta^- + \bar{\nu}$$

On the average, six antineutrinos are emitted before a stable nuclide is reached. Here ^{144}Pr and ^{89}Y have significantly longer half-lives, and are therefore considered stable.

Uranium-238 is an isotope which is abundant in the fuel, and is converted into fissionable plutonium isotopes such as ^{239}Pu and ^{241}Pu during reactor operation via neutron capture. An example of this capture reaction is shown below:

$$U^{238} + n \rightarrow U^{239} + \gamma \rightarrow Np^{239} + \beta^- + \bar{\nu} \rightarrow Pu^{239} + \beta^- + \bar{\nu}$$

The antineutrinos emitted during this capture reaction are usually negligible when compared to the antineutrinos emitted following fission. In addition to these

thermal neutron reactions, ^{238}U also undergoes fission when bombarded by fast neutrons, but the energy released during such reactions contributes only up to 10% of the total energy released from the core. There will be antineutrinos emitted following the decay of fission products produced during this fast fission and they will contribute only a small portion of the total antineutrino emission from a reactor.

Although ^{235}U is the major fissile isotope in a low-enriched uranium (LEU) fueled light water reactor (LWR) during the beginning of the cycle, over time it is depleted via fission and neutron capture by ^{238}U results in the formation of fissile plutonium isotopes such as ^{239}Pu and ^{241}Pu. These plutonium isotpes contribute significantly to the fission rate during the later stages of the core cycle. Similar to ^{235}U, these isotopes also produce fission products and energy upon fission. The fission products from the plutonium isotopes also undergo negative beta decay, but the energy spectrum of the antineutrinos released is slightly different from that of the ^{235}U fission products.

By measuring these antineutrinos, the fission rate in the reactor, and consequently the operating reactor power level, can be estimated. Further, for a known power level, the antineutrino signature measured may also provide the details of the nature of the fission products and the isotopic composition of the fuel in the reactor.

1.1 Antineutrino Spectra

Antineutrinos are mass-less (million times lighter than an electron), neutral particles, making them nearly impossible to shield and hence they provide an effective

means for verifying reactor operations. However, the same properties that make them difficult to shield also make them difficult to detect. The interaction cross-section of these particles is very small and it poses a challenge in achieving good detector efficiencies for antineutrino detectors. Figure 1 shows the energy spectrum of antineutrinos produced following the fission of the four major fissioning isotopes in light water reactors: ^{235}U, ^{239}Pu, ^{238}U and ^{241}Pu.

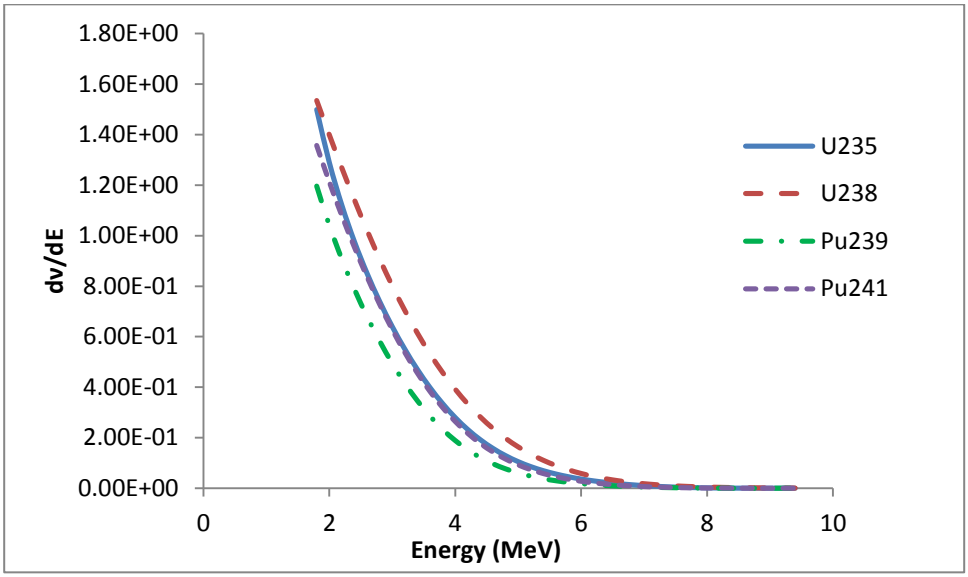

Figure 1.1: Antineutrino spectra from fission (Bowden, 2008)

The ordinate of this graph is the number of antineutrinos emitted (dv) per unit energy (dE), and the abscissa is the antineutrino energy. The size of the energy bin is .2 MeV. The antineutrinos emitted with energies below 1.8 MeV are not included in the spectrum shown because they are undetectable with current detector technologies (Bowden et al., 2008).

1.2 Antineutrino Detection

The physics of antineutrino detection has evolved over the past five decades to the state where it is now feasible to employ this technology for reactor safeguards. There has been continued research in developing antineutrino detectors around the globe. A description of the most notable experiments is included in Table 1.1.

Table 1.1: Antineutrino detection experiments

Country	Experiment	period	Detector configurations	Description
USA	Cherenkov detector	1953	Cadmium laced liquid scintillator	First neutrino measuring experiment
	SONGS1 detector	2003 -2007	1 cm^3 gadolinium (Gd) laced liquid scintillator	Successfully monitored the power level of the SONGS reactor
Russia	Rovno	1993 - present	A new Gd liquid scintillator using linear alkyl benzene solvent is under development	Showed correlation between antineutrino flux, thermal power and fuel burn-up.
France	CHOOZ	2003-2005	5 ton liquid scintillator at 1 km from the core.	Set limits on the neutrino oscillation parameters responsible for changes in reactor neutrinos.
	Double CHOOZ	2011 - 2012	Two 10 ton detectors, one at 100 m and other at 1km from reactor core.	To measure accurately the θ_{13} interaction angle of neutrinos emitted from a PWR.
Japan	Kamland	2002 - present	1000 tons of liquid scintillator in central japan.	Detected antineutrinos from a number of reactors at an average distance of 180 km.
Brazil	Angra	2006 - present	50 ton and 500 ton liquid scintillators.	Yet to be deployed.

In this research, emphasis will be placed on detector development in the USA because these detectors have been developed for non-proliferation applications. A brief discussion of the operating principles of the SONGS1 detector and other detection mechanisms that are being investigated is given below. A more detailed discussion of the different detectors can be found in the literature (Alex Misner, 2008) (Bowden, 2008).

The SONGS1 detector was developed by Sandia National Laboratories (SNL) and Lawrence Livermore National Laboratory (LLNL) in a joint effort. The detector was deployed at the San Onofre Nuclear Generating Station (SONGS) between 2003 and 2006. This detector is based on the inverse beta decay reaction of antineutrinos with protons. Most antineutrino detection experiments have been based on this reaction. The process of inverse beta decay is shown in the equation below.

$$\bar{\nu} + p \rightarrow \beta^{+} + n$$

The antineutrino spectra measured using the inverse beta decay process for the two major fissile elements ^{235}U and ^{239}Pu differ significantly. The difference in the number of measured antineutrinos arises because of the difference in the energy of antineutrinos emitted following the fission of ^{235}U and ^{239}Pu. On average, this results in 1.92 and 1.45 detectable antineutrinos per fission for ^{235}U and ^{239}Pu, respectively (Cribier, 2007).

In the SONGS1 detector, an active volume consisting of 0.64 tons of gadolinium-doped liquid scintillator is enclosed in stainless steel cells. The detector, shown in Figure 2, is surrounded by a shield made of water/polyethylene to eliminate

neutron-gamma background and a plastic scintillator to veto cosmic muons. Further, the atmospheric background cosmic rays are effectively shielded by placing the detector in the tendon gallery of SONGS unit 2 below ground at a distance of 25m from the reactor core.

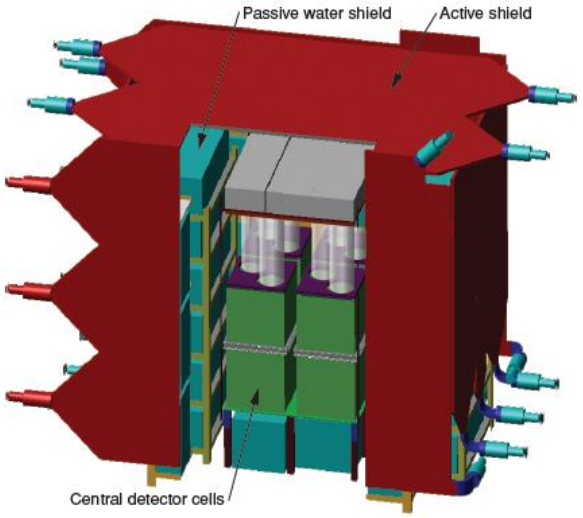

Figure 1.2: SONGS detector schematic (Bowden, 2008)

The antineutrinos from the reactor interact with the proton-rich scintillator and the positron product deposits its kinetic energy and then annihilates with an electron, emitting γ-rays that are then detected. This process is rapid and produces what is referred to as the "prompt signal". Product neutrons are absorbed by an isotope that is added to the detection medium (dopant) which then decays one or more times, emitting γ-rays. This occurs on the order of tens of microseconds after the positron annihilation and is referred to as the "delayed signal" (Bernstein, Wang, et al.). Figure 3 illustrates these reactions as they occur in a detector. Antineutrino detectors look for these two

events to happen in coincidence, which has the added benefit of reducing the background signal.

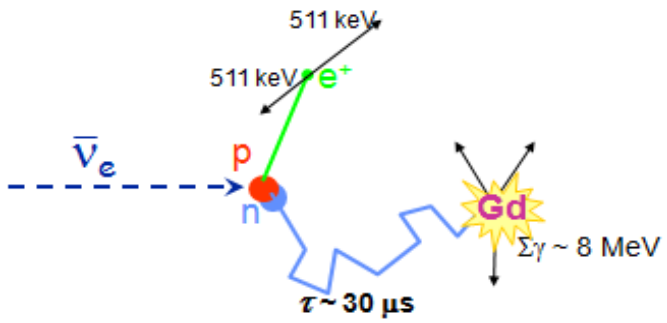

Figure 1.3: Inverse β – decay in an antineutrino detector (Alex Misner, 2008)

The interaction cross-section for the inverse beta decay process is very small (of the order of 10^{-44} cm^2 for the SONGS detector) and depends on the energy of the incident antineutrino spectrum, as shown in Figure 4. The efficiency of the SONGS1 detector was around 10%. However, the detector successfully transmitted real time data to the labs and was able to detect the occurrence of a SCRAM within 5 hours with a 99% confidence. Over a 24 hour period, the power of the reactor was monitored at a precision of about 8%. Also the decrease in the antineutrino rate due to fuel depletion (transition from ^{235}U to ^{239}Pu) when operated at constant power, and increase in the antineutrinos following refueling (replacing depleted assemblies with fresh UO_2 assemblies), were successfully monitored (Bowden, 2008).

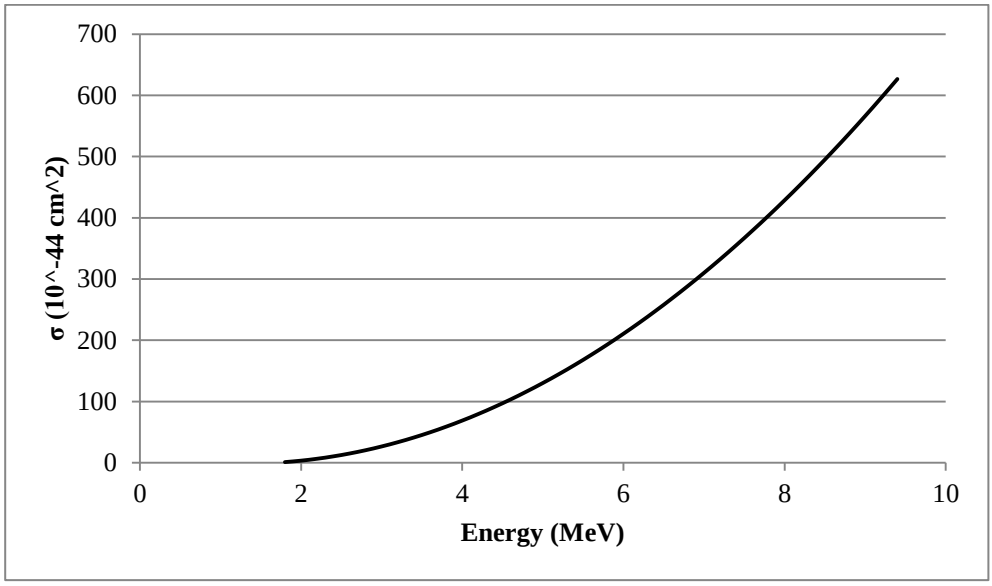

Figure 1.4: Change in detector cross section with mean antineutrino energy (Alex Misner, 2008)

It is essential to acknowledge the fact that the two parameters of interest, power and fuel inventory, both cannot be determined independently with the current detection technology. That is, to determine the fuel inventory, it is essential to have the power history of the plant. But, if the detectors could resolve the detected antineutrino energy spectrum, it would become feasible to monitor these parameters independently. Antineutrino detectors based on coherent scattering of the nuclei when interacting with antineutrinos may be able to provide the energy information, but such detectors are still in the primitive stages of development (Bernstein et al., 2002).

1.3 Previous Simulations

In parallel with detector development, there have been increasing efforts to predict the antineutrino signature of reactors under different operating conditions using reactor simulation tools. It is unsafe and impractical for a reactor to be operated under

all the possible diversion scenarios that are of concern for the IAEA. To effectively employ antineutrino detectors to monitor power reactors around the globe, it is essential to have a well-established database of antineutrino signatures for the various possible operating and diversion scenarios of the different reactors. Also, the efficiency of the detectors required to detect the change in antineutrino signature for the various situations that are of concern may be determined from the predicted antineutrino rates. Simulation results are very helpful in setting goals for future antineutrino detector development.

There have been some notable previous efforts to simulate the diversion of material from a nuclear reactor. The CINDER software package was used to predict antineutrino emission rates from a reactor core in a study conducted by Los Alamos National Laboratory (LANL) (Nieto, Hayes, Teeter, Wilson, & Stanbro, 2003). In this study the core was simulated with one third of the fuel fresh, one third of the fuel having been burned once, and one third of the fuel being twice-burned at the beginning of the cycle. Several diversion scenarios with extra fuel being replaced during refueling were also simulated. In the first scenario, an extra 10% of the fuel in addition to the normal 33% was replaced with fresh fuel. In the second scenario, an extra 100% of the fuel in addition to the normal 33% was replaced. The results of the study showed that there was less than 1% change for the first scenario, while the second scenario produces a 5% higher antineutrino emission rate at the start of the next cycle.

This study was followed by a similar zero-dimensional simulation (no spatial dependence is considered) of a reactor core by Sandia National Labs (SNL) and

Lawrence Livermore National Laboratory (LLNL) using the LEOPARD code (Bernstein 2006). This simulation was intended to predict the change in antineutrino rate for the SONGS (San Onofre Nuclear Generating Station) unit 2 Reactor. This study was performed before the deployment of the SONGS 2 detector. There was no diversion scenarios modeled in the study.

Following the SONGS detector experiment, a study was conducted using the ORIGEN-ARP (Oak Ridge Isotope Generation – Automated Rapid Processing) fuel depletion code that is available within the SCALE package (Alex Misner, 2008). ORIGEN-ARP was used to model the SONGS reactor core to compute the antineutrino source terms and the detector response. The simulation results agreed with the experimental results within the uncertainty of the observed data. The study also investigated diversion scenarios for a LEU core with Westinghouse 17*17 assemblies and a MOX core model developed by Purdue University. Each of these models was simulated under three different diversion scenarios. The study concluded that the scenario in which the reactor operated at 105% of nominal power generated a large enough difference in antineutrino emission rate to be detected for both the LEU and MOX cores. The scenario that involved the replacement of fresh fuel with fertile targets produced differences of less than 1% for both core types. However, the removal of plutonium-rich assemblies produced a more pronounced result. In the MOX case, the diversion scenario resulted in a nearly 3% increase in the antineutrino emission rate over the normal baseline case at the beginning of the cycle, but for the LEU core the difference was smaller because less plutonium was removed. Differences were observed

in the antineutrino emission rates of cores fueled with LEU and MOX. The MOX core emitted 15% fewer antineutrinos per megawatt of thermal energy produced than the LEU core.

1.4 Need for Additional Simulation Capabilities

Calculations using the lattice-level ORIGEN-ARP requires the power history of individual assemblies. This information is, in general, not available. It is essential to perform core-level, three-dimensional reactor simulations to develop a database of antineutrino predictions during normal and diversion scenarios such that the counts from the detector could be used to interpret valuable information about the status of the reactor. Further, antineutrino source terms may be dependent on different factors such as fuel assembly type, enrichment, power density, reactor type, fuel loading pattern, etc. It is essential to know if there are significant changes in the antineutrino signatures with changes in the different reactor parameters. In this study, CASMO and SIMULATE, LWR simulation codes from Studsvik Scandpower Inc. are used to compute the antineutrino rate for several light water reactor designs. The main emphasis is on determining the changes in antineutrino signature for a PWR (Pressurized Water Reactor) and MASLWR (Multi Application Small Light Water Reactor). This study also investigates the difference in antineutrino source terms for different fuel loading patterns and diversion scenarios involving MOX fuel. It also includes the simulation of the SONGS unit 2 reactor for benchmarking.

1.5 Research Objectives

The objectives of this research are to determine the antineutrino rates of different reactor types under different scenario and compare their results. This thesis focuses on the simulations performed for LWR models using CASMO and SIMULATE. This work answers address the following research questions:

1. How accurately can CASMO and SIMULATE be used for antineutrino source term predictions of light water reactors?
2. How different are the antineutrino source terms for a fresh core with LEU fuel, an equilibrium core refueled with LEU and a MOX loaded core?
3. Can the prediction of antineutrino signatures be improved by taking into account the radial and axial variations of the source terms?
4. How different are the antineutrino signature of a LWR and a SMR (Small Modular Reactor)?

2 Methods

2.1 Reactor Simulation Tools

Modern nuclear reactor design depends heavily on various mathematical models of the nuclear fission chain reaction applied to core analysis using digital computers. The computer programs that simulate the nuclear reactor core have been developed as a result of extensive research and testing at various nuclear laboratories around the world. These computational tools are focused on simulating various aspects of the nuclear reactor core. Codes can be classified into four major categories as follows (Dudertstadt & Hamilton, 1976).

1) Cross section library processing codes
2) Multi group constant generation codes
3) Static design codes
4) Time dependent design codes
    a) Depletion codes.
    b) Fuel cycle analysis.
    c) Reactor kinetic analysis.

In this research, the focus is on the simulation of an operating reactor and therefore depletion codes along with the necessary cross section processing and group constant generation routines are used. During reactor operation, the composition of fuel assemblies will change and fission products will be formed. While operating a reactor, these changes in fuel composition must be understood to predict the reactivity, flux, multiplication and other critical parameters that

determine the proper operation of the reactor. The study of the interaction of the core power distribution with the time-dependent production or depletion of nuclei in the core is known as *depletion* or *burn-up* analysis. In a depletion calculation, the material composition and flux distribution during the operational life of the core are calculated. Depletion codes solve a coupled system of rate equations describing isotope concentrations and the neutron balance equation describing the core criticality. There are a significant number of variables involved and solutions are required at many points in time.

A variety of tools are available to perform depletion analyses of reactors and each has its own advantages and disadvantages. All the reactor simulation tools have either a deterministic approach or stochastic approach to the neutron transport problem. The performance of the tool is evaluated based on a number of parameters such as accuracy, speed and scalability (ability to perform complex three – dimensional core level calculations as well as simple one-dimensional pin-level calculations). In this research, a deterministic code that solves the transport equation is used for fuel assembly (or lattice) simulation and to generate the group constants. To perform the reactor core simulation, a deterministic code that solves the neutron diffusion equation is used.

2.1.1 Lattice Level Simulation

The assembly models for light water reactors (LWRs) are simulated using CASMO-4 (Edenius, Ekberg, Forssén, & Knott, 1995) - a multi-group two-dimensional transport code developed by Studsvik Scandpower Inc, and is written in

FORTRAN 77. It is used for burn-up calculations on boiling water reactor (BWR) and pressurized water reactor (PWR) assemblies or pin-cells. The code can accommodate geometries of cylindrical fuel rods of varying composition in a square pitch. Rods such as those containing fuel alone, fuel and gadolinium, individual burnable absorber rods, and cluster control rods can be accurately modeled by CASMO-4.

The code first calculates the macroscopic group cross sections for each distinct region within the pin-cell known as the micro-regions. The nuclear data library ENDF/B-6 is an integral part of the code and has cross sections in 70 and 40 energy groups. It uses an equivalence theorem to calculate the effective cross sections in the resonance energy region for important resonance absorbers. The screening effects between different pins are treating using Dancoff factors that are calculated automatically by CASMO-4. These cross sections are then used in micro group calculations to obtain the neutron energy spectra. The micro group calculations are performed for each pin type present in the assembly using the method of collision probabilities. The micro group spectra are then used to obtain the broad group cross sections for all the pin cells. The details of the spectra are then used for energy condensation and spatial homogenization of pin cells. A 2D macro group calculation is then performed using the homogenized pin-cells and cross-sections in 40 energy groups. The solution of this calculation would yield the neutron spectra for the final energy condensation of cross-sections that would be used for two-dimensional, heterogeneous transport calculation using the method of characteristics. This calculation is performed in a maximum of 8 energy groups.

The solution of the two-dimensional transport calculation gives the multiplication factor (k-eigenvalue) and flux distribution of the assembly. The effects of leakage are included by modifying the results of the transport calculation with the fundamental mode buckling. The isotopic depletion as a function of exposure is calculated for each fuel pin and for each region containing a burnable absorber. A predictor-corrector approach is then used for the burn up calculation. The depletion is initially calculated using the spectra from the previous step and the depletion is calculated at the end of the step using the new spectra calculated for that step. An average of these two number density calculations is then used as starting values for the next step. CASMO-4 also performs branch calculations automatically via the S3C input card. When the S3C card is used, CASMO-4 automatically performs calculations for a complete set of core conditions that would be used in the core level calculation. The depletion and branch calculations performed by CASMO-4 for a single assembly are used to generate the lattice physics parameters. These parameters include the cross sections, nuclide concentrations, pin power distributions and other nuclear data used as input to the SIMULATE-3 program, which performs the core analysis for light water reactors. Figure 2.1 shows the flowchart of the CASMO 4 methodology in performing the burn-up calculation.

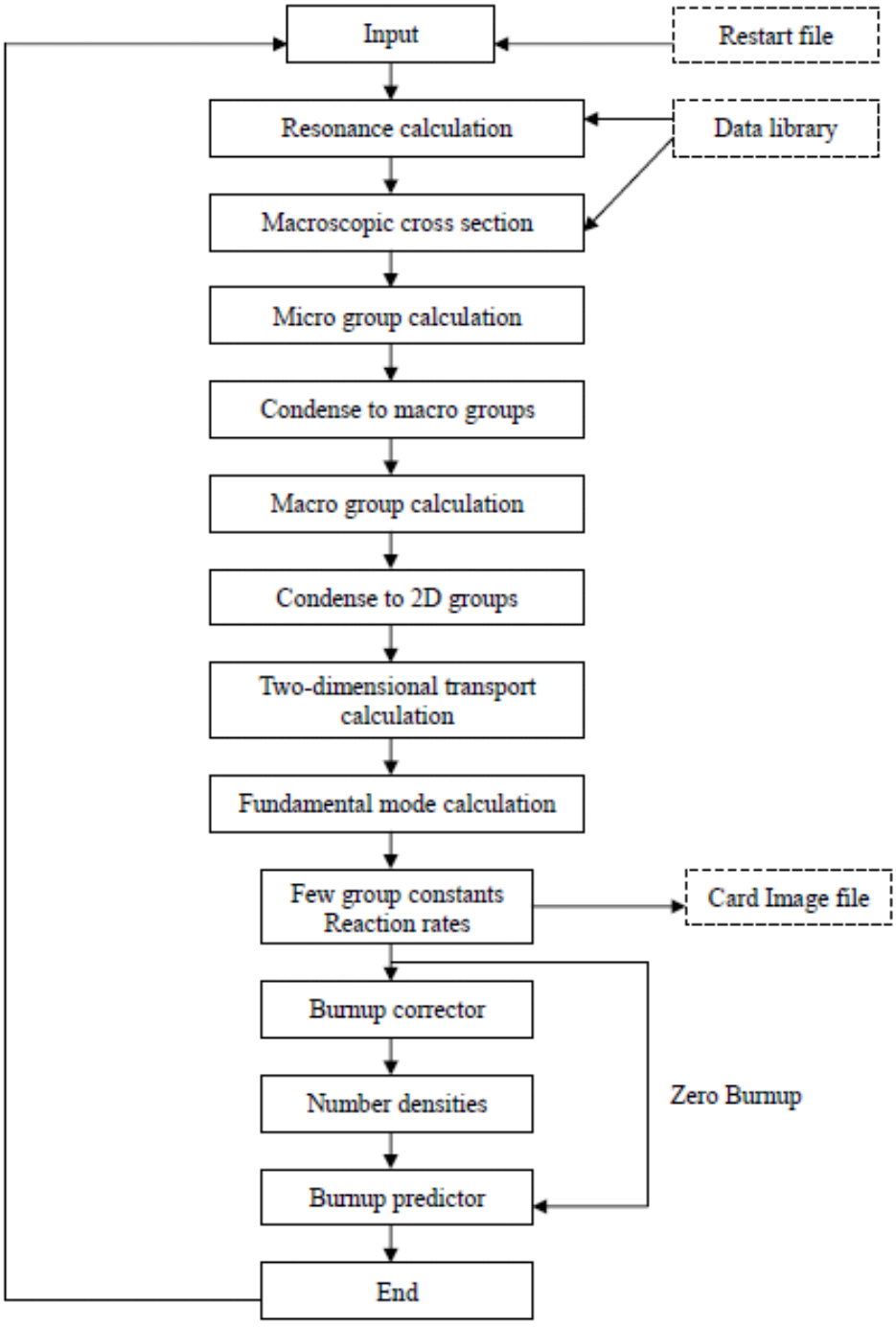

Figure 2.1: CASMO-4 depletion calculation flow chart (Edenius et al., 1995)

2.1.2 Core Level Simulation

Studsvik Scandpower Inc also supplies the SIMULATE-3 code. It is a two-group, three-dimensional nodal diffusion program based on the NRC staff-approved QPANDA neutronics model that employs fourth-order polynomial representations of the intra nodal flux distributions in both the fast and thermal neutron groups. This code is based on the modified coarse mesh (nodal) diffusion theory calculation technique, coupled with thermal hydraulic and Doppler feedback. This program explicitly models the baffle/reflector region, eliminating the need to perform higher order fine mesh calculations. It also includes the necessary routines that solve the two-group neutron diffusion equation, perform fuel assembly homogenization, calculate explicit reflector cross-sections, deplete isotopes, recalculate macroscopic cross-sections and reconstruct pin powers.

In order to ensure flux continuity at nodal interfaces and perform an accurate determination of pin-wise power distributions, SIMULATE-3 uses assembly discontinuity factors that are pre-calculated by CASMO-4. These factors are related to the ratio of the nodal surface flux in the actual heterogeneous geometry to the cell averaged flux in an equivalent homogeneous model, and are determined for each energy group as a function of exposure, moderator density and control-rod position.

The two-group model solves the neutron diffusion equation in three dimensions and assembly homogenization is performed using the flux discontinuity correction factors from CASMO-4 to combine the nodal flux shape and the assembly heterogeneous flux distribution. The flux discontinuity factors are also applied to the

baffle/reflector region in both radial and axial directions to eliminate the need for normalization or other adjustment at the core/reflector interface.

The SIMULATE-3 fuel depletion model uses tabular and functionalized macroscopic or microscopic, or both, cross sections to account for fuel exposure without tracking the individual nuclide concentrations. Depletion history effects are calculated by CASMO-4 and then processed by the CMS-LINK code for generation of the cross-section library used by SIMULATE-3. SIMULATE-3 can be used to determine the fuel isotopics and two group fluxes for individual assemblies in three dimensions. It also calculates control rod worth and moderator, Doppler, and xenon feedback effects (Christian & Allen, 2003).

2.1.3 MOX treatment in SIMULATE-3

Radial power distributions in MOX-fueled reactor cores are difficult to predict accurately using standard nodal analysis models. Much of the difficulty arises because of the larger (2-3 times) thermal absorption cross sections for MOX assemblies than those in neighboring UO_2 assemblies. This large mismatch gives rise to steep thermal flux gradients and large spectral interactions between MOX and UO_2 assemblies. In 1990, a series of new models was introduced into versions of SIMULATE-3 that permit application of the code for MOX-fueled cores. Initial applications were for low plutonium concentrations (3.0 - 5.0% total) and later it was applied to high plutonium concentrations (up to 12% total plutonium). The newer models employed advanced nodal methods that use two dimensional, non-separable

expansions of polynomial and hyperbolic functions to represent the two-group flux instead of the usual transverse leakage approximation method (Palmtag, 1997).

The accuracy of the SIMULATE-3 MOX models has been verified by benchmarking with color-set (2x2) results obtained on several reference MOX cores using an extended version of CASMO-4 which permits quarter core calculations with the detailed heterogeneous geometry with fuel pins, absorber pins, coolant, etc, while still using the detailed transport model. This model typically involves 128 azimuthal angles, 3 polar angles, 0.1 cm ray spacing, and 16 energy groups (Dean, 2009).

2.1.4 Cross-Section Library and Fission Product Treatment

CASMO-4 uses a data library called the E6LIB based on the ENDF/VI Library. The library contains cross sections, decay constants and fission yields for 337 materials, most of which are individual nuclides. Cross sections for complex materials are obtained by combining the cross sections of the constituent elements. It also tracks all the heavy nuclides and fission products chain in the ENDF/VI library. The selected structure and yield values give yield sums for each fission precursor very close to 2.0, the theoretical yield value as there are two fission products formed per fission of the parent nuclei. The burn-up chains are made linear and 24 separate fission products, 2 pseudo-fission products and 17 heavy nuclides are tracked (Umbarger & DiGiovine, 1992).

2.2 Models

In this work, three different reactor types have been modeled. The first is a Combustion Engineering (CE) type PWR core operated by San Onofre Nuclear Generating Station (SONGS). The second is a Multi-Application Small Light Water Reactor (MASLWR) core. The third is a Westinghouse type PWR core. Each of the models is explained below.

2.2.1 SONGS Model

In order to validate the accuracy of the CASMO/SIMULATE codes in determining the antineutrino source terms of a reactor, the SONGS reactor unit 2 is modeled. The SONGS antineutrino detector was deployed during operating cycle 13 of the reactor. The core map, initial enrichment, exposure and power histories of fuel assemblies in the core of cycle 13 were obtained from SONGS and used in the simulation and comparisons are made with the observed antineutrino detection rates. The operational core data provided by SONGS is proprietary to Southern California Edison Company. Other reactor parameters such as flow density, control rod structure, number of burnable poison rods and their composition, core height, reflector material, etc., are obtained from the final safety analysis report (FSAR) of the SONGS reactor (SCE & SDG&E, 1978)

The SONGS Unit 2 reactor is a Combustion Engineering (CE) type reactor with a maximum power rating of 3650 MWt. It has 217 fuel assemblies of the Westinghouse 16x16 type with large control rods (4 pins wide). A typical 16x16 fuel assembly layout is shown in Figure 2.2.

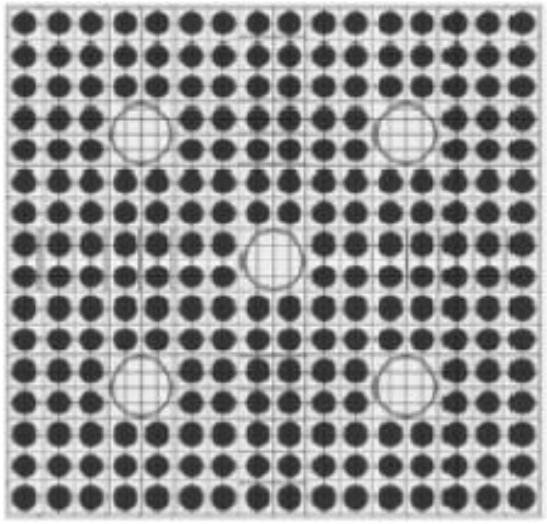

Figure 2.2: **Westinghouse CE 16*16 PWR assembly**

Roughly half the core was loaded with fresh fuel assemblies while the remaining were once burnt and twice burnt assemblies. The core layout of the SONGS reactor is shown in Figure 2.3. The green assemblies represent fresh fuel while the yellow and red assemblies represent once burnt and twice burnt assemblies. A three-dimensional full core representation was modeled and depleted at full power in SIMULATE-3. The calculations were performed with 12 nodes per assembly axially and 2 nodes per assembly in the radial (x and y) dimensions. An iterative boron search was employed to maintain the multiplication factor (k - eigenvalue) at 1. All the control rods are in the fully withdrawn position.

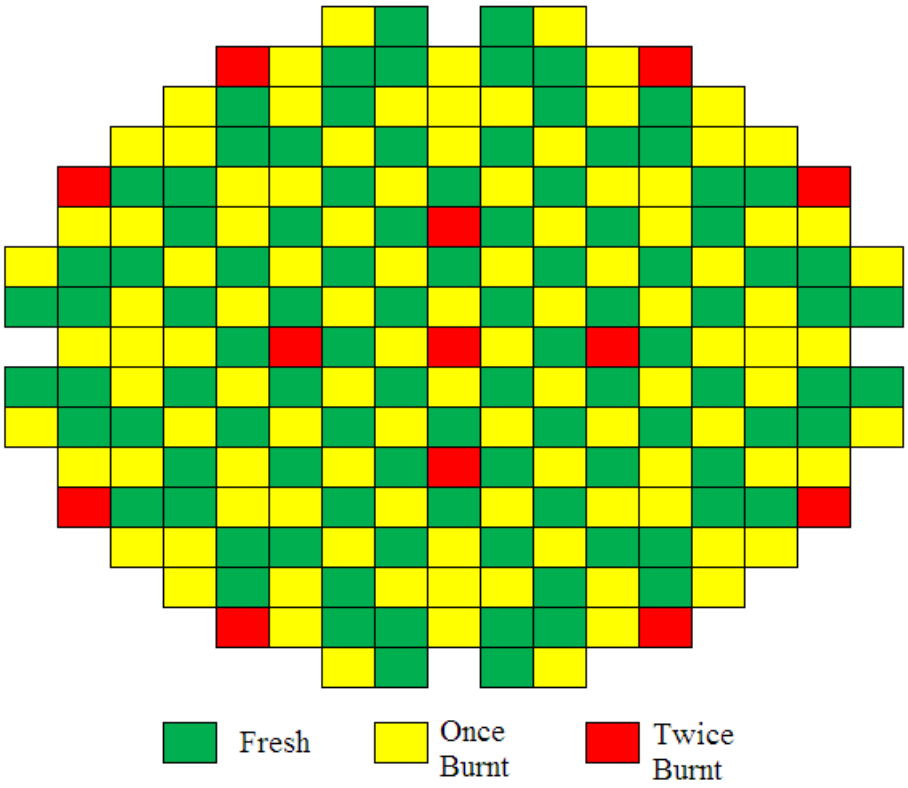

Figure 2.3: SONGS core map (Alex Misner, 2008)

2.2.2 MASLWR Model

According to the International Atomic Energy Agency (IAEA), there may be as many as 96 or as few as 43 small modular reactors (SMRs) in operation by 2030, none of them in the USA (WNA, 2011). Some SMRs are proposed to be exported to developing countries with small electrical grids and/or installed in remote locations, which might cause serious proliferation risks. To reduce security costs, the U.S. Nuclear Regulatory Commission is looking to designers to incorporate security into the SMR designs, but this has yet to be done. Antineutrino detectors are being considered for this purpose. MASLWR (Multi Application Small Light Water Reactor) is a 45 MWe modular reactor design developed at Oregon State University

in partnership with Idaho National Laboratory. The core design had 24 fuel assemblies of the Westinghouse 17x17 design with an axial length of 165cm - half the height of a typical PWR core (Soldatov & Palmer, 2009).

Four different fuel assemblies are used, two containing LEU and the other two containing MOX fuel. The description of the different assemblies is given in Table 2.1. The reactor grade (RG) plutonium composition was assumed equal to the plutonium composition of reprocessed fuel with an initial ^{235}U enrichment of 4.5% and average burn-up of 40 MWD/kg HM. The weapons grade (WG) plutonium composition was taken from an ORNL report (Gehin et al., 2004).

Table 2.1: Assembly types used in MASLWR core

No	Assembly Type	Description
1	LEU - UO_2	4.5 wt% ^{235}U /U
2	LEU - UO_2	2.5 wt% ^{235}U/U
3	RG - MOX	5 wt% Pu/HM with 64.9 wt% ^{239}Pu /Pu
4	WG - MOX	5 wt% Pu/HM with 91.7 wt% ^{239}Pu /Pu

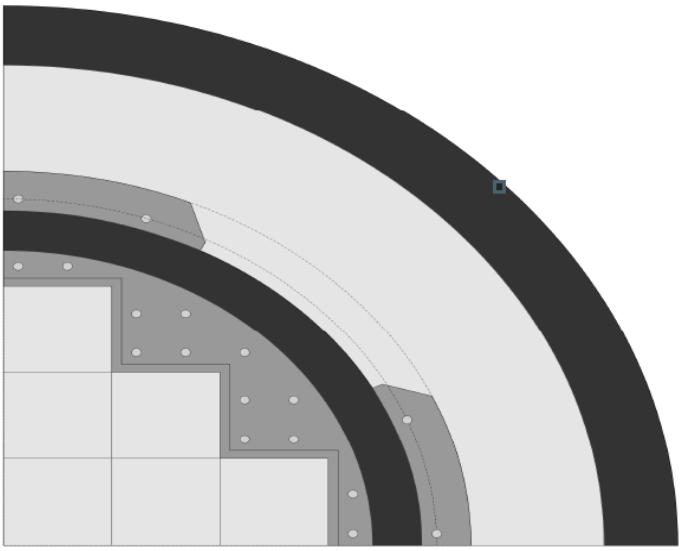

Figure 2.4: **Quarter core model for MASLWR** (Soldatov & Palmer, 2009)

A MASLWR core with twenty four fuel assemblies is modeled and depleted at a full power rating of 150 MWt. The physical dimensions of the fuel assemblies, axial and radial reflectors and other core operating parameters are obtained from previous MASLWR simulations. Figure 2.4 shows the schematic of a quarter section of the MASLWR core.

To evaluate the antineutrino signature of the core for normal and diversion scenarios, a number of different fuel cycles are simulated. Initially, the core is loaded with fresh 4.5 wt% enriched UO_2 at the periphery and 2.5 wt% enriched UO_2 at the center. Beginning from the second cycle, half of the depleted assemblies are replaced by fresh fuel assemblies. The core reached an equilibrium cycle length after the third cycle when refueled with 4.5 wt% UO_2 assemblies at the end of cycles 1 and 2. An OUT-IN loading pattern was adopted for these cycles. Once an equilibrium core is reached, the fourth cycle was simulated for five different cases as shown in Figure 2.5. The type of fuel assembly is denoted by ^{235}U enrichment for LEU assemblies. The MOX assemblies are denoted by RG and WG for reactor grade and weapons grade fuel, respectively.

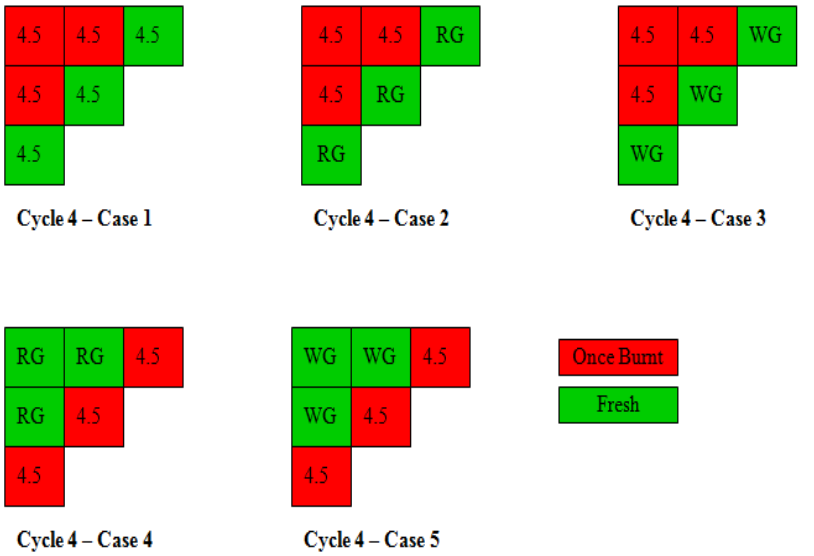

Figure 2.5: Fuel loading pattern for different cases of cycle 4

Case 1 is the normal refueling condition in which the twice burnt assemblies at the center of the core are removed, the once burnt assemblies are moved to the center, and fresh LEU assemblies are loaded at the periphery. Case 2 represents a similar refueling pattern with reactor grade (RG) MOX fuel instead of LEU fuel. Case 3 is a similar refueling pattern with weapons grade (WG) MOX fuel. In cases 4 and 5, instead of moving the once burnt assemblies from the previous cycle to the center, the fresh assemblies are loaded at the center with RG and WG MOX, respectively. The different core cycles will help to identify the differences in antineutrino signature between normal operating conditions and two potential diversion scenarios. The first diversion scenario is the one in which the power plant receives WG MOX fuel for utilization in the reactor but operates on normal LEU assemblies, thereby diverting weapons grade material. The second scenario is a similar situation in which RG MOX assemblies are loaded in the core instead of WG MOX fuel.

The third potential diversion scenario considered is the removal of 8kg of plutonium from the once burnt assemblies with higher plutonium concentration from the core and replacing them with fresh assemblies. In this case the once burnt assemblies with high plutonium content are replaced with fresh 2.5 wt% enriched UO_2 assemblies.

2.2.3 Westinghouse Model

A three dimensional core model of a Westinghouse type reactor with 193 fuel assemblies is also considered. This model is simulated for four different cases, each with different fuel configurations. In case 1, a fresh core with burnable poisons is simulated to emulate the first cycle of a reactor core. The nuclear design parameters of the Sequoyah reactor unit 1 are obtained from its FSAR (TVA, 1983). The assemblies were all of Westinghouse 17x17 type. The core has three regions, with ^{235}U enrichments 2.1%, 3.1 % and 2.6 %, respectively. The fuel assemblies have burnable poison rods to control the excess reactivity. The burnable poison rods have a boron concentration of 12% and are inserted in the control rod/guide thimble pins. Figure 2.6 shows the quarter core model of the Sequoyah reactor with 56 fuel assemblies. The number of burnable poisons in each assembly is also displayed. The arrangement of burnable poisons in each assembly in the core is taken from the Sequoyah FSAR. All the other reactor parameters such as power density, reflector compositions, control rod structure, coolant flow density etc are also taken from the Sequoyah reactor FSAR and are included in Appendix A. The core was depleted at full power throughout the cycle. This simulation will be used to compare the

antineutrino source terms of a fresh core with an equilibrium core and MOX cores that are simulated later.

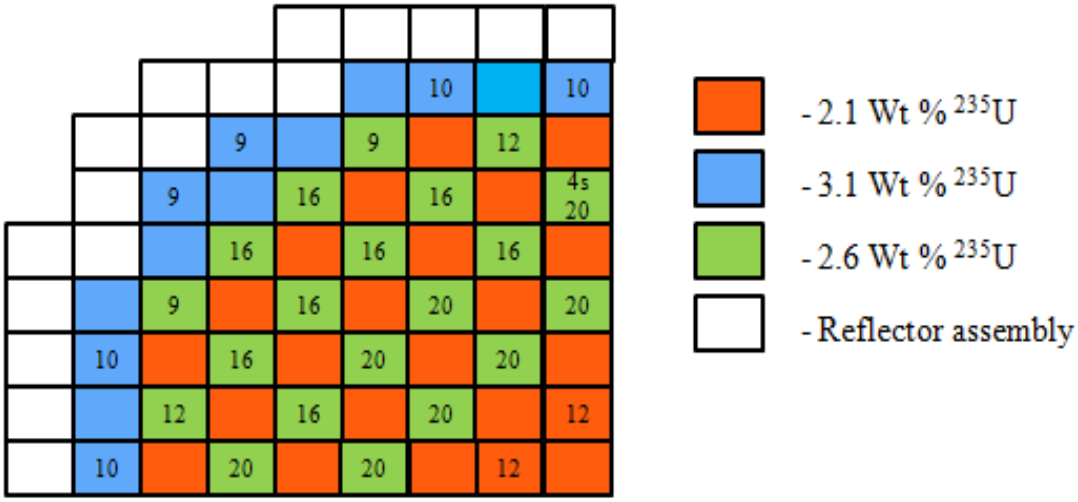

Figure 2.6: Sequoyah quarter core model with number of burnable poisons

In case 2, the simulation is performed using a quarter core model similar to the Sequoyah core, but with four different fuel regions: two LEU regions and two MOX regions. The fuel properties are taken from a Nuclear Regulatory Commission (NRC) report for an UO_2/MOX benchmark core by Purdue University (Kozlowski & Downar, 2006). Figure 2.7 shows the quarter core map of the MOX core. It has 14 MOX and 42 LEU assemblies. The two LEU regions had ^{235}U enrichments of 4.2% and 4.5%, respectively. The two MOX regions had a total plutonium enrichment of 4.3% and 4.0% respectively. The numbers displayed in the assemblies denote the exposure in GWD/MT for each assembly. From the plutonium vector used in the MOX assemblies, the fuel is identified as WG MOX and is slightly different than that used in the MASLWR simulations. The plutonium and uranium vectors for the MOX assemblies are given in Appendix A.

The assemblies had burnable poisons in both LEU and MOX regions. The LEU assemblies used 104 integral fuel burnable absorber rods (IFBA) that provide reactivity control during the initial stages of burn up, while the MOX assemblies used 24 wet annular burnable absorber (WABA) rods inserted in the control rod/guide tube locations. Figures 2.8 and 2.9 show the pin configurations for the LEU and MOX assemblies.

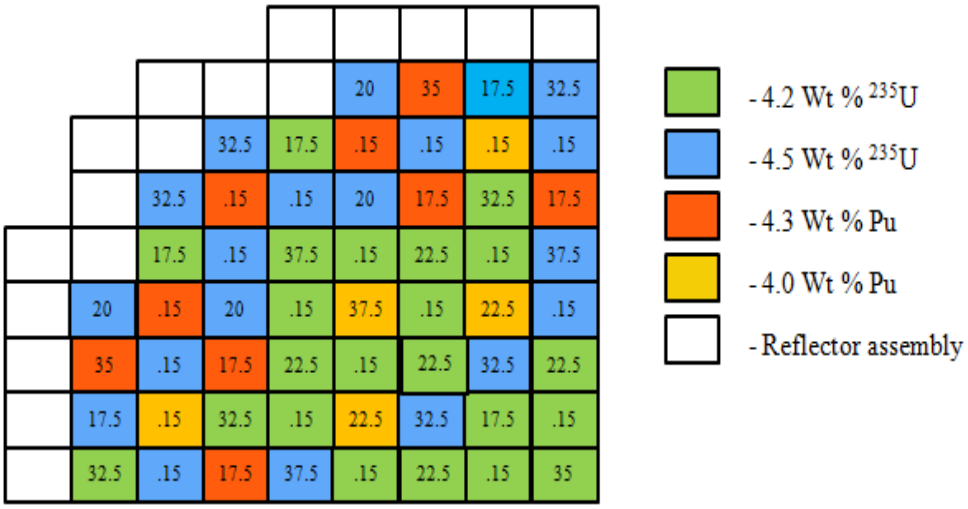

Figure 2.7: PWR UO_2/MOX core with exposure values

In case 3, the simulation was performed using the same core layout as the previous MOX core, but the plutonium vector was changed to match the RG MOX composition used in the MASLWR simulations. These simulations will help to see the differences in antineutrino signature between a core with WG MOX and RG MOX.

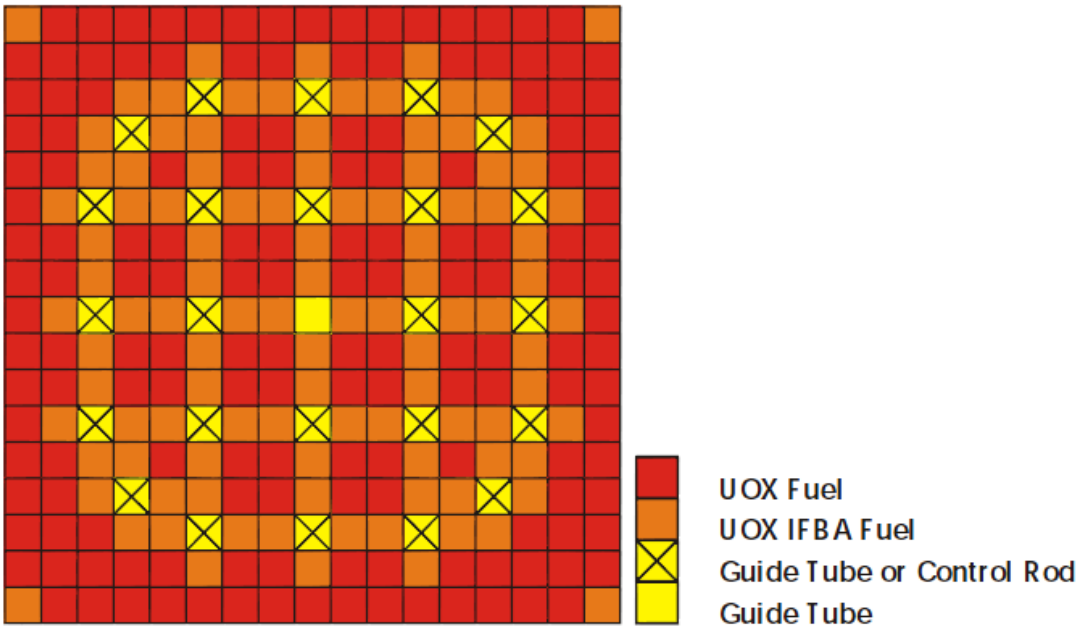

Figure 2.8: Westinghouse 17x17 LEU assembly with 104 IFBA pins (Kozlowski & Downar, 2006**)**

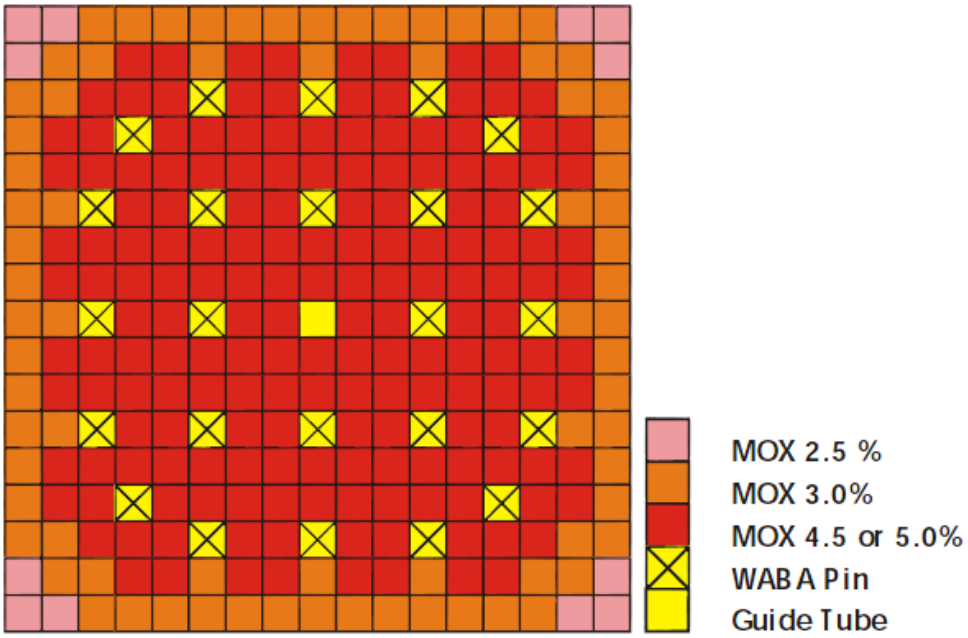

Figure 2.9: **Westinghouse 17x17 MOX assembly with 24 WABA pins** (Kozlowski & Downar, 2006)

In case 4, the core layout of the MOX core was retained but the MOX assemblies are replaced with LEU assemblies of the same composition present in the rest of the core. The 4.3% Pu assemblies are replaced with 4.5% ^{235}U assemblies and

the 4.0% Pu assemblies are replaced with 4.2% ^{235}U assemblies to replicate a LEU equilibrium core. All the core parameters such as flow density, thermal power, etc. remain the same for cases 2, 3 and 4 and were also obtained from the NRC report for UO_2/MOX benchmark core.

2.3 Methodology

In this section the software tools and methods used to determine the antineutrino source terms of the reactor from the results of the simulation tools are discussed.

2.3.1 Fission Rates

The initial step in determining the antineutrino spectrum of the reactor is to calculate the fission rates of each individual fissile isotope present in the fuel. The formula for finding the fission rates is

$$R_i = \sum_{a=1}^{n} N_{i,a} \sum_{g=1,2} \sigma_{i,a,g}\, \varphi_{i,a,g}$$

i – Isotope (^{235}U, ^{238}U, ^{239}Pu,^{241}Pu)

a – Assembly number (1, 2, 3… n)

g –Energy group (1, 2)

R_i – Fission rate (fissions sec^{-1})

$N_{i,a}$ – Number of atoms

$\sigma_{i,a}$ – Microscopic cross sections (cm^2)

$\varphi_{i,a}$ - Total flux (neutrons cm^{-2} sec^{-1})

The two group fluxes in three dimensions and the isotopics of individual fissile isotopes for each assembly are obtained from SIMULATE-3 at each exposure point. The fission cross-sections of the isotopes are not directly available as an edit from SIMULATE-3 and therefore as a first approximation, the fission cross sections are computed from CASMO-4 calculations of each assembly in the core for average operating conditions.

2.3.2 Fission Cross sections

To find the fission cross sections of individual fissile isotopes in the fuel, the fission reaction rates of each micro region in the fuel assembly are determined from CASMO-4 output. The fission rates are edited in two groups, fast and thermal, with energy group boundaries [10 MeVto .62 eV] and [.62 eV to 0 eV], respectively. Once the fission rates of the individual isotopes are known, the microscopic cross sections are obtained by determining the number densities of the isotopes, the volume of the segment as calculated in CASMO-4 and the two group fluxes. The cross sections are calculated for each micro region at every burn-up stage and the average cross section for each stage is then stored in a spreadsheet. This is repeated for every segment in the core and the cross sections are stored with the appropriate segment tag.

The next step in determining the fission cross sections of the individual assemblies in the core is to determine the specific exposure of each assembly in each axial node for every time step as calculated by SIMULATE-3. Once the exposure values of the assemblies are known, the appropriate cross section for every assembly

at each axial node is interpolated from the cross section spreadsheet. Having found the fission cross sections, the fluxes and the number of atoms of each isotope, the fission rate by isotope for every assembly and for every axial node is calculated. All the calculations and processing are done using a C++ code. The flowchart for the code is shown in Figure 2.10.

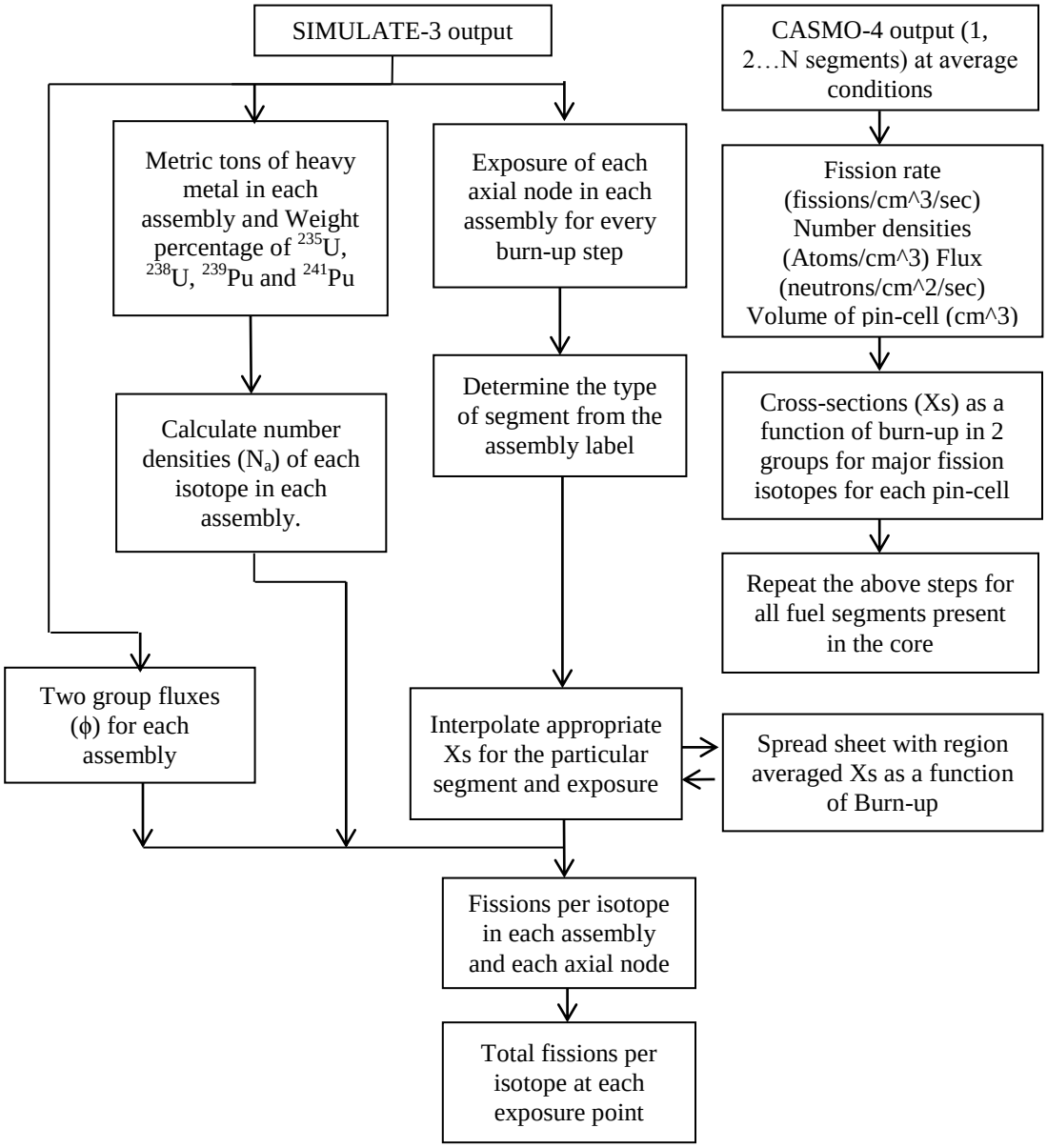

Figure 2.10: Flowchart for calculating fission rates from simulation output

2.3.3 Antineutrino source terms

There have been a number of different experiments conducted to measure the antineutrino spectra of fission products from the major fission isotopes (^{235}U, ^{239}Pu , ^{241}Pu) in a nuclear reactor (Avignone III & Greenwood, 1980) . Using the experimental results and from the knowledge of fission product yields, beta branching ratios and binding energies, mathematical correlations have been devised to predict the antineutrino spectrum emitted and associated relative errors. The correlations are provided either as a formula or table that can be used to convert from fission rate to spectral antineutrino emission rate. In this research, the correlations from the latest work on antineutrino predictions by Huber and Schwetz are used (Huber & Schwetz, 2004).

2.3.4 Detector Response

To benchmark the SONGS reactor core simulation results with observed results during the SONGS antineutrino detection experiment, the detector response is calculated from the simulated antineutrino source terms. The detector properties such as proton density, intrinsic efficiency, detector volume and standoff distance from the core are taken from the literature (Bowden et al., 2008). The cross sections for the inverse-beta decay reaction have been extensively studied and predictions of the cross sections as a function of antineutrino energy are available (Vogel & Beacom, 1999).

In previous simulation efforts, the detector response is calculated assuming the reactor core to be a point source located at a fixed distance from the detector. But, since SIMULATE can perform three-dimensional simulations of the core, the three-

dimensional coordinates of every axial node in every assembly in the core with respect to the detector location (origin) are determined using the core dimensions, detector location and node definitions. The distance between every node in the core and the detector is then found and used in determining the detector response. The total detector response thus obtained is then compared to the detector response assuming a point source such that any improvement in accuracy by performing a three dimensional simulation can be assessed. All the calculations are performed using a C++ code. The formulas for determining the detector response using the point source method and three-dimensional method are given below.

Point source method:

$$\mathrm{C(t)} = \sum_{a=1}^{N_{assem}} \sum_{n=1}^{N_{nodes}} \sum_{g=1}^{G} N_{v,a,n,g}(t)\sigma_g \Delta E_g \frac{N_p \varepsilon}{4\pi D_{avg}^2}$$

Three-dimensional method:

$$\mathrm{C(t)} = \sum_{a=1}^{N_{assem}} \sum_{n=1}^{N_{nodes}} \frac{N_p \varepsilon}{4\pi D_{a,n}^2} \sum_{g=1}^{G} N_{v,a,n,g}(t)\sigma_g \Delta E_g$$

C(t) – Detector count rate (counts/day)

N_p – Detector proton density (cm^3)

$D_{a,n}$ – Standoff distance between detector and node n in assembly a (cm)

D_{avg} – Average distance between detector and center of the core (cm)

ε – Detector efficiency

σ_g – Antineutrino interaction cross section for energy group g

$N_{v,a,n,g}(t)$ – Antineutrino emission rate at time t

ΔE_g – Width of antineutrino energy group g

g – Antineutrino energy group,

a –Fuel assembly index

n – Axial node index

3 Results

3.1 SONGS benchmark results

3.1.1 Comparison of total fission rates

The SONGS unit 2 reactor operated at a total power rating of 3640 MWt for a period of 650 days during cycle 13. Considering a mean fission energy of 202.5 MeV per fission (MG Sowerby, 2011), a rough estimate of the total fission rate yields 1.12E20 fissions per second. The total fission rates calculated from the simulation results during the entire cycle are presented in Figure 3.1. The total fission rates from the simulation varied between 1.15E20 and 1.12E20 fissions per second.

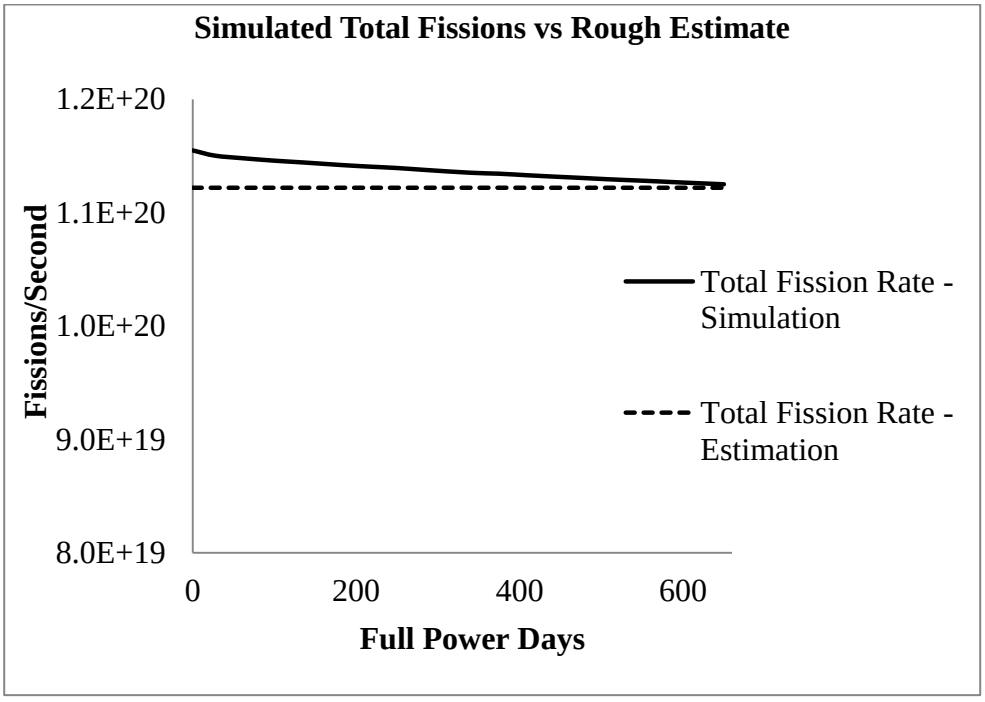

Figure 3.1: Comparison of total fission rates from simulation with rough estimate for SONGS unit 2, cycle 13

3.1.2 Comparison of fission rates by isotopes

The fission rates of the major fission isotopes ^{235}U, ^{239}Pu , ^{238}U and ^{241}Pu calculated from SIMULATE-3 output are compared with the predicted fission rates found in the literature (Bowden et al., 2008). Figure 3.2 shows the calculated fission rates of the major fissile isotopes from the SIMULATE-3 output. Figure 3.3 shows the same as presented in the literature. They show similar trends throughout the cycle for all the four major fissile isotopes. But their magnitudes are different due to the differences in power level and fuel enrichment. The SIMULATE-3 simulation was done at the exact conditions in which the core operated during cycle 13, while the simulation in the literature was done at core conditions quoted in the SONGS FSAR.

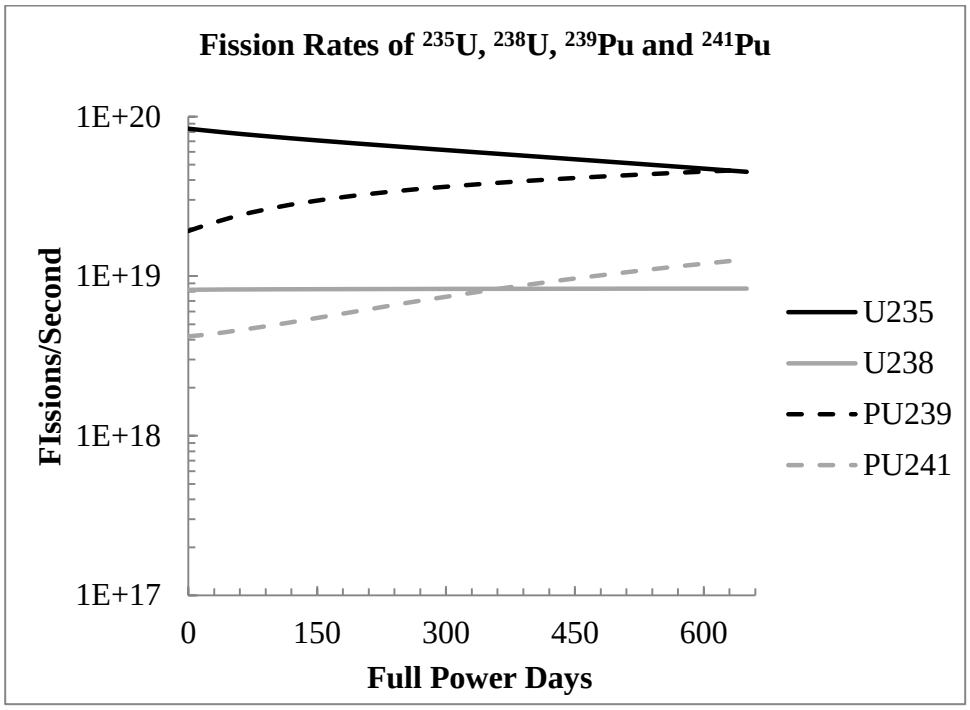

Figure 3.2: Fission rates by isotope for SONGS unit 2, cycle 13, calculated from SIMULATE-3

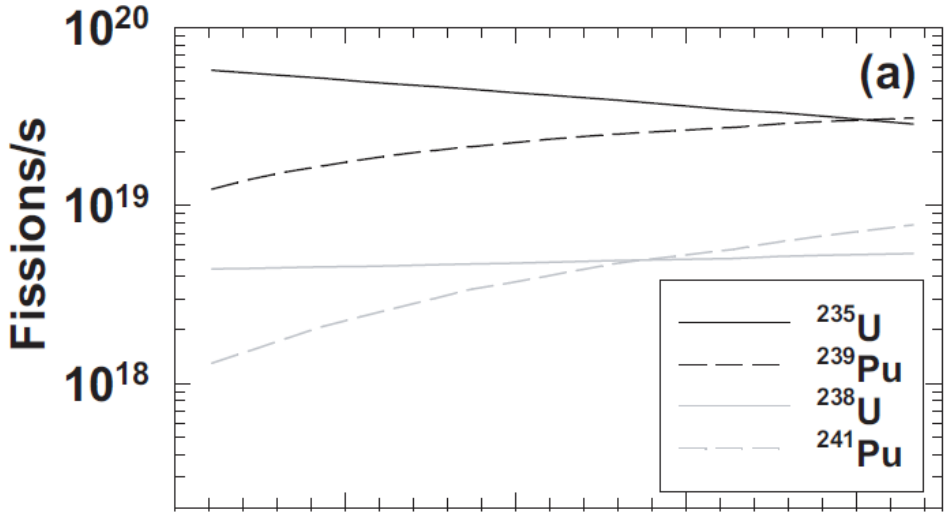

Figure 3.3: Predicted fission rates by isotope for SONGS unit 2 (Bowden et al., 2008)

3.1.3 Antineutrino signature

Figure 3.4 shows the antineutrino source terms calculated from SIMULATE-3 results for cycle 13. The number of antineutrinos emitted per fission for the major fission isotopes ^{235}U, ^{239}Pu , ^{238}U and ^{241}Pu are calculated using semi empirical formulas (Huber & Schwetz, 2004). The errors associated with the predictions are also calculated using a six parameter fit (Huber & Schwetz, 2004). Figure 3.4 also shows the corresponding total fission rates for cycle 13. The total change in antineutrino source terms calculated between the beginning and end of the cycle is about 10%.

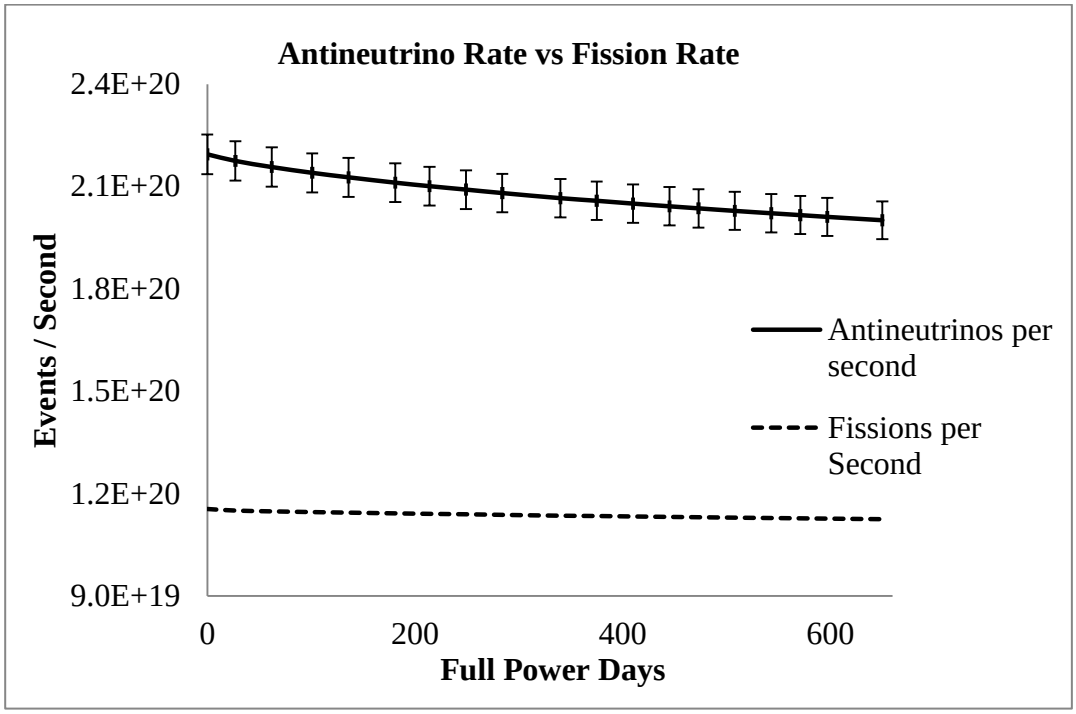

Figure 3.4: Calculated antineutrino signature along with the errors and fission rates for SONGS unit 2, cycle 13

3.1.4 Detector response

The detector response is calculated for each assembly and each axial node individually and summed up to yield the total detector response. The detector properties used are obtained from (Bowden et al., 2008; Alex Misner, 2008). Figure 3.5 shows the detector response calculated from the simulation results for different combinations of detector efficiency (ε) and stand-off distance between the center of the core and the detector (D). The reasoning behind the different efficiency values used is given in Table 3.1.

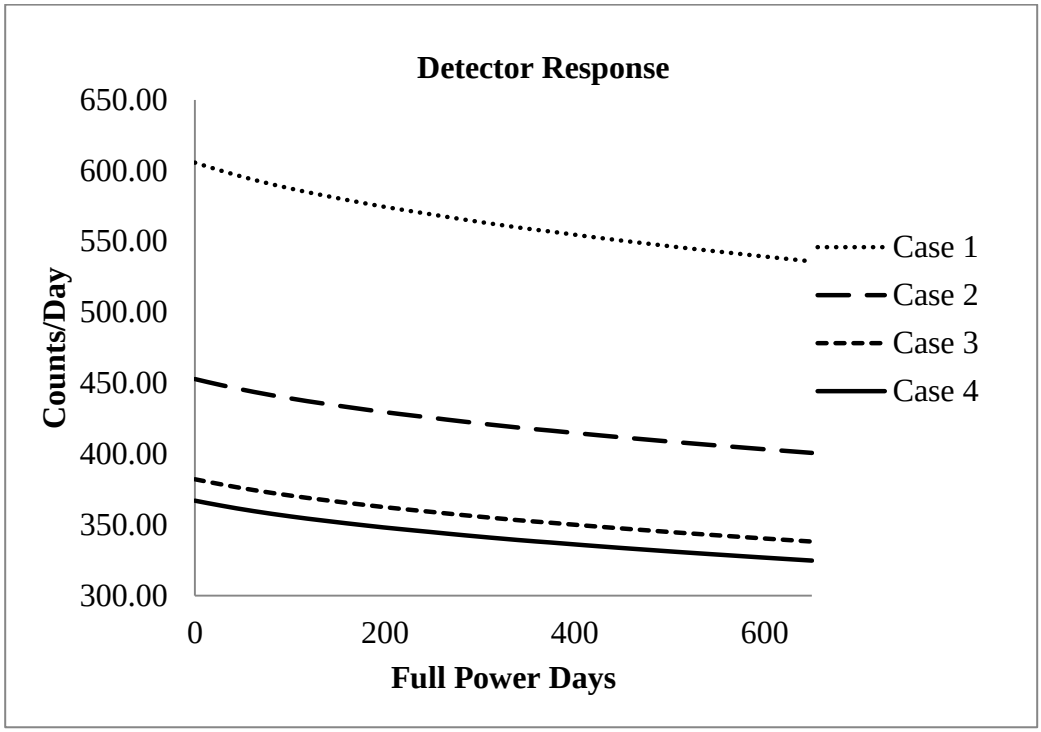

Figure 3.5: Detector responses at different efficiency, stand-off distance combinations of the SONGS 1 detector

Table 3.1: Efficiency and stand-off distance combinations and justification

Case	ε (%)	D (cm)	Description
1	10.7	2450	Overall efficiency and stand-off distance as predicted in (Bowden et al., 2008).
2	8.05	2450	1 out of 4 cells in the detector did not work. (Bowden et al., 2008)
3	6.75	2450	Actual efficiency after accounting for losses. (Bowden et al., 2008)
4	6.75	2500	Stand-off distance used in previous simulation (Alex Misner, 2008)

Figure 3.6 shows the comparison of calculated counts from SIMULATE 3 output with the measured counts from SONGS 1 detector and the predicted counts from previous simulation using ORIGEN-ARP (Bowden et al., 2008). The detector response calculated using the efficiency and stand-off distance values from case 4 are used for this comparison. Figure 3.6 also shows the uncertainty of the detector in

measuring the antineutrinos. It could be seen from the plots that for most data points the simulation results lie within the uncertainty of the detector. Table 3.2 shows the counts calculated from SIMULATE-3 output along with the relative error when compared to the measured counts. Table 3.2 also shows the relative error in the counts calculated due to uncertainties present in antineutrino parameterization from fission rates, and counting statistics (Alex Misner, 2008). The error between measured and calculated counts lies within the error due to uncertainty in the calculation.

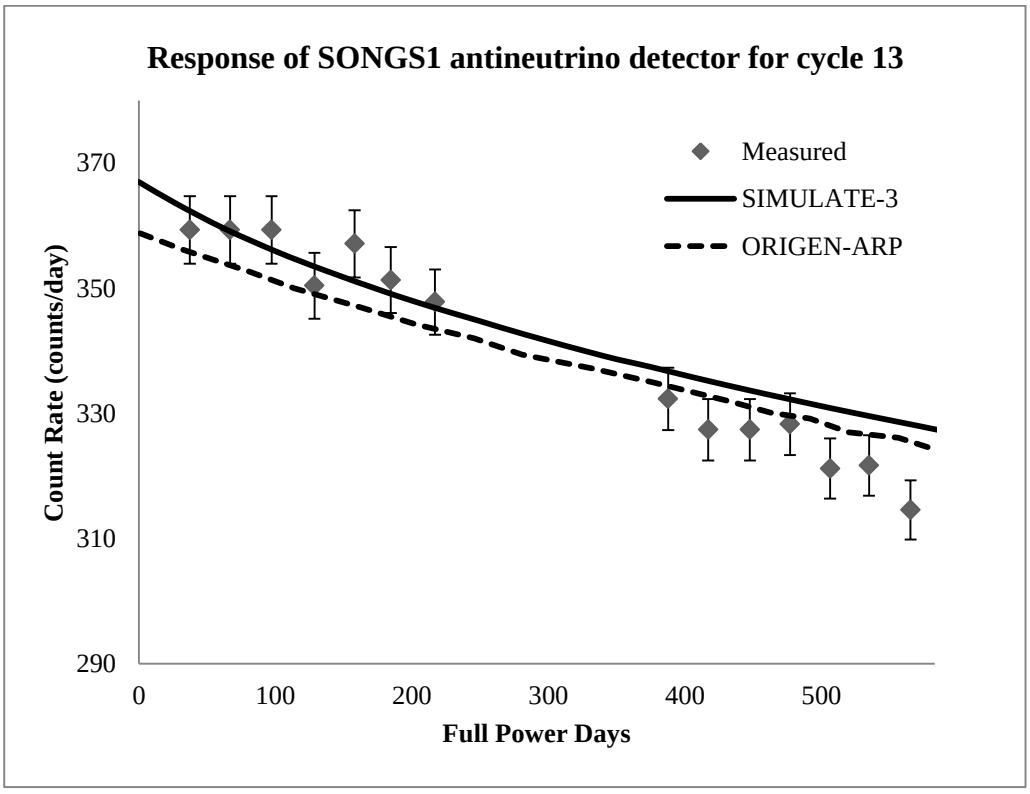

Figure 3.6: Detector response of SONGS 1 detector from experiment and calculation

Table 3.2: Relative error between measured counts and calculated counts and relative error due to uncertainties in calculating the detector response.

Days	Calculated Counts	Relative error between measured and calculated counts	Relative error in calculation
37	362	0.01	0.05
67	360	0.00	0.05
97	357	0.01	0.05
129	354	0.01	0.05
158	352	0.02	0.05
185	350	0.00	0.05
217	347	0.00	0.05
388	336	0.01	0.05
417	334	0.02	0.05
448	333	0.02	0.05
477	331	0.01	0.05
506	330	0.03	0.05
535	328	0.02	0.06
565	327	0.04	0.06

It was also verified that considering the reactor core as a point source from the detector yields results that are similar to the results calculated from a three-dimensional representation of the core. Table 3.3 shows the counts obtained by both methods. However, this similarity can be attributed to the uniform core loading. Three-dimensional representation of the core fission rates would yield better results for scenarios where control rod insertions and asymmetric loading patterns are present. The case of asymmetric loading is illustrated later in one of the MASLWR diversion scenarios.

Table 3.3: Comparison between counts calculated from the three dimensional representation of the core and by considering the core as point source

Days	Counts from three-dimensional calculation	Counts from point source calculation
0	367	367
27	364	363
62	360	359
101	356	355
136	353	352
181	349	349
214	347	346
249	345	344
284	343	342
340	339	339
375	337	337
410	336	335
445	334	333
473	332	332
508	331	330
543	329	329
571	328	327
597	327	326
650	325	324

3.2 MASLWR results

3.2.1 Comparison of Equilibrium Core with MOX cores

Figure 3.7 shows the total antineutrino rate calculated for the normal LEU loaded equilibrium core plotted against the antineutrino rates calculated for four MOX loaded cores. The difference in antineutrino rates observed between RG MOX (cases 2 and 4) and WG MOX (cases 3 and 5) loaded cores are very minimal with the RG MOX cores emitting 3% higher antineutrinos than the equivalent WG MOX core**.** This

difference is due to the difference in antineutrinos emitted by the fissions of the plutonium isotopes ^{239Pu} and ^{241Pu}(Alex Misner, 2008). ^{241Pu} emits slightly more antineutrinos than ^{239Pu} and hence the core with a higher percentage of ^{241Pu} emits more antineutrinos. The antineutrino rate of the equilibrium core (case 1) is higher than the MOX cores, because of the higher 235U content in the core. The MOX cores with fresh MOX assemblies loaded at the center (case 4 and 5) emit fewer antineutrinos than the cores loaded with MOX assemblies loaded at the periphery (case 3 and 4). This is mainly due to the higher percentage of plutonium fission in the core. The average fission rate of all the cases at BOC was found to lie within 1% of the rough estimate value of 4.6E18 fissions per second calculated at a power rating of 150 MWt.

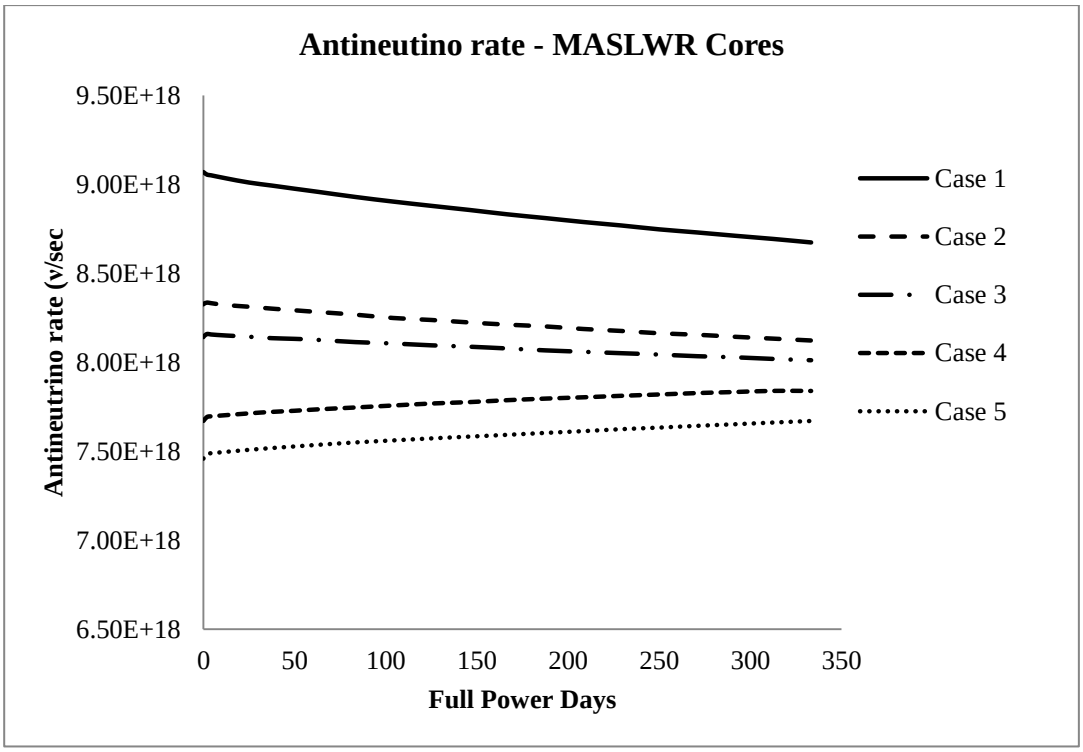

Figure 3.7: Antineutrino source terms of equilibrium MASLWR core compared with MOX loaded cores

3.2.2 Response of SONGS1 detector to MASLWR core

Table 3.4 shows the increase in count rates for the SONGS1 detector with decreasing stand-off distance from the core. For the SONGS1 detector to be able to record similar counts from a MASLWR equilibrium core as that of the SONGS core, the stand-off distance had to be reduced from 2500cm to 650 cm. Figure 3.9 shows the detector response calculated for the five cases of MASLWR cores simulated at a stand-off distance of 650cm and an over-all detector efficiency of 10.7%.

Table 3.4: Relationship between stand-off distance and detector counts at beginning of cycle (BOC)

Efficiency (%)	Distance (cm)	Counts at BOC
10.7	2500	24
10.7	1000	151
10.7	750	269
10.7	650	358
10.7	600	420
10.7	500	605

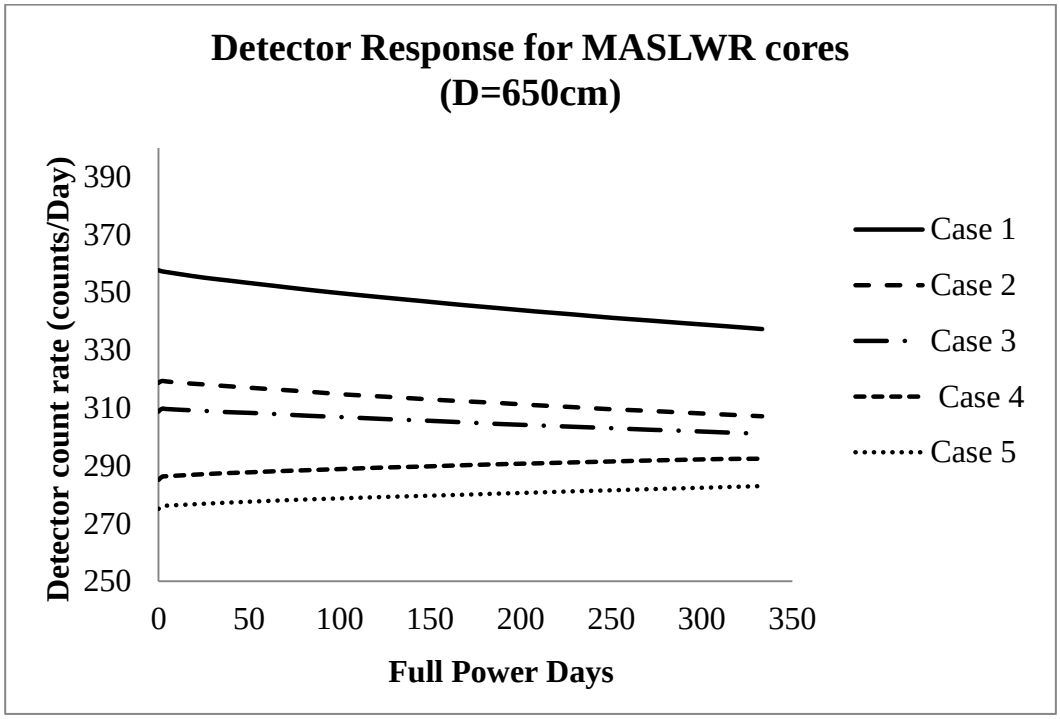

Figure 3.8: Detector response of SONGS 1 detector for MASLWR at a stand-distance of 650 cm

The maximum difference in counts is observed between cases 1 and 5 and is about 83 counts at BOC. The error due to counting statistics and antineutrino spectrum calculation is approximately ±18 counts.

3.2.3 Removal of 8 kg plutonium from MASLWR core

The removal of 8kg plutonium from the normal equilibrium core was simulated at two different time intervals from BOC. The first interval was at 167 full power days into the cycle. Eight once burnt assemblies from the center of the core with high plutonium content were replaced by fresh UO_2 assemblies with a 235U enrichment of 4.2%. The second interval was chosen at 291 full power days into the cycle. Seven once burnt assemblies with high plutonium content are replaced with UO_2 assemblies. Figure 3.9 shows the variation in antineutrino spectrum from the normal cycle for the two

diversion scenarios. An increase of 3.8% in the antineutrino rate is observed immediately following the diversion at 167 days. Similarly, an increase of 4.6% in the antineutrino rate is observed immediately following the diversion at 291 days. The increase in antineutrino rate when recorded by the SONGS1 detector at a stand-off distance of 600 cm would show an increase of 19 and 17 counts respectively for the 167 days and 291 days diversion scenarios. This change in counts falls within the range of counting statistics, meaning that it would not be distinguishable from normal detector fluctuations.

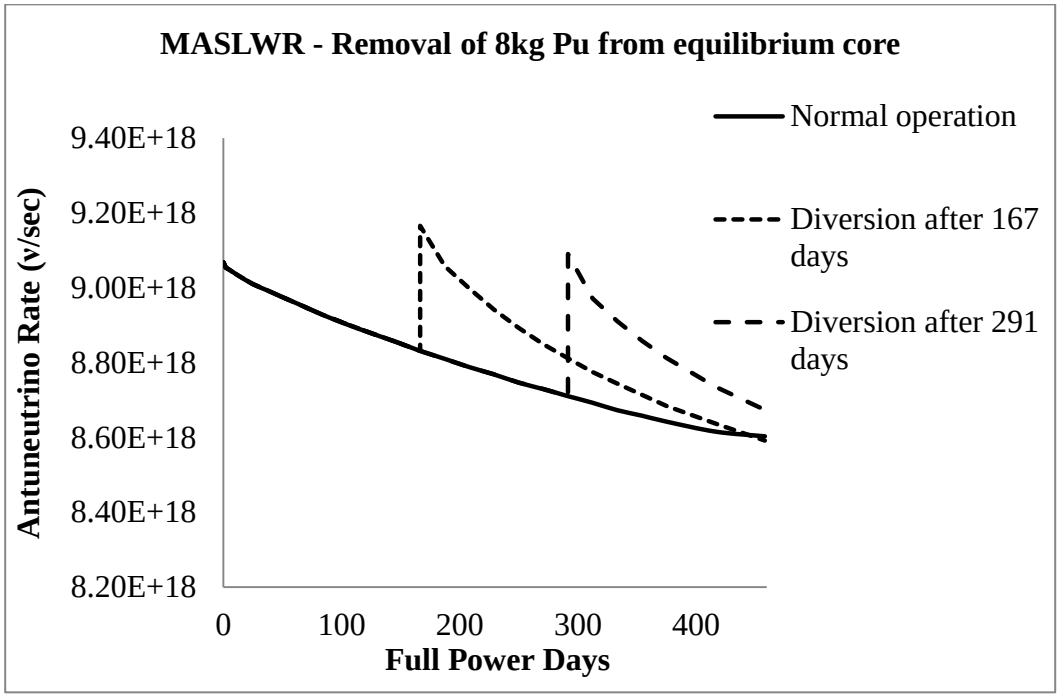

Figure 3.9: Changes in antineutrino spectrum of the MASLWR core for the removal of 8kg plutonium at different time intervals from BOC

3.2.4 Detector response of an asymmetrically loaded core

The removal of 8 kg plutonium after 291 days by removing seven assemblies from the core was simulated twice with different assemblies being removed from the

core. The purpose of these two simulations is to predict changes in count rate calculated from the antineutrino source terms expressed in three-dimensions to the counts calculated assuming the core to be a point source of antineutrinos. In the first simulation, seven assemblies are removed such that three assemblies from the south-east (SE) quarter, two assemblies from north-east (NE) quarter and two assemblies from south-west (SW) quarter of the core are replaced by fresh assemblies. In the second simulation, the same numbers of assemblies are removed from the SW and NE quarter, while the remaining three assemblies are removed from north-west (NW) quarter of the core. With the detector assumed to be located south of the center of the core, the detector counts calculated for the two simulations using the direct point source method and three dimensional method is shown in Figure 3.10.

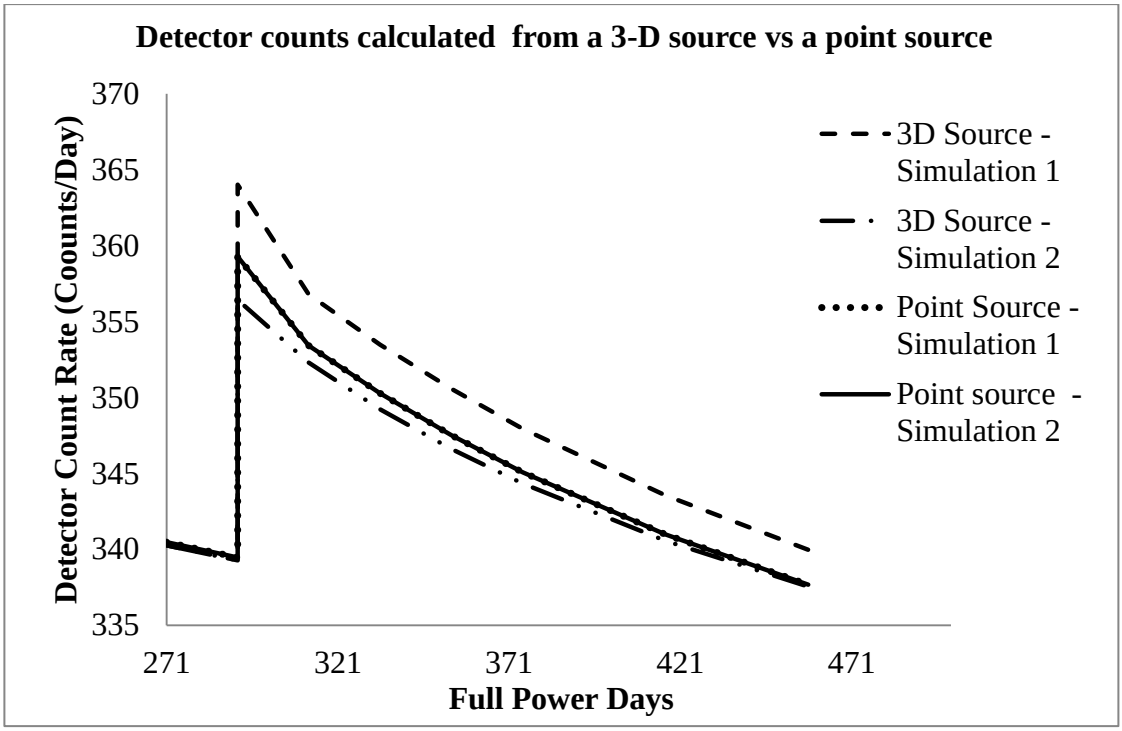

Figure 3.10: Comparison of detector counts calculated from a three-dimension calculation vs counts calculated by point source method

This plot shows that the total detector counts calculated by the point source method are exactly the same for both simulations. But, there is a noticeable difference between the counts calculated using the three-dimensional method. As expected, the counts for the first simulation were higher due to the fact that the detector is located closer to the SE region of the core from which the maximum number of assemblies are replaced with fresh fuel. For the second simulation, more assemblies are exchanged from the NW region and hence the lower detector counts. Immediately after the diversion, the difference in counts observed between the two scenarios is around 9 counts. However, this difference will go up for larger cores with a increased assymmetry.

3.3 Westinghouse results

Figure 3.12 shows the comparison of antineutrino rates per fission calculated from the simulation of a fresh LEU core with burnable poisons (case 1), a partially MOX loaded core with two batches of burnt fuel and one batch of fresh fuel, and an equilibrium LEU core with one batch of fresh fuel and two batches of burnt fuel (case 4). For the MOX cases simulations were performed for both WG MOX (case 2) and RG MOX fuel (case 3). The results show there is very minimal difference between RG MOX and WG MOX fuels. It is also observed that the antineutrinos per fission emitted for the equilibrium LEU core are 2.7% higher than that of the MOX core at BOC. When compared with the fresh LEU core, the equilibrium LEU core emitted 4.7% fewer antineutrinos. Figure 3.11 shows that the curves for the fresh LEU core and equilibrium LEU core intersect towards the middle of the cycle, indicating the formation of plutonium in the fresh core. The error introduced by the uncertainties in

calculating the antineutrino spectrum from fission rates is about 2.2% and therefore determining the type of fuel in the core would depend highly on the sensitivity of the detector.

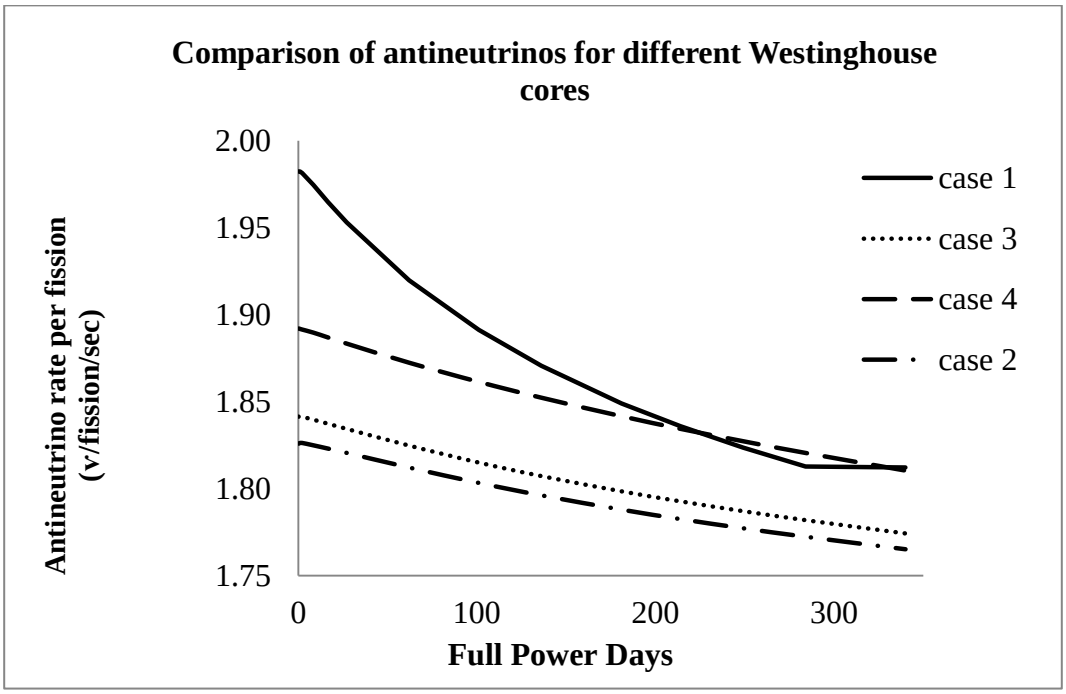

Figure 3.11: Comparison of antineutrinos per second for different cases of Westinghouse core simulation

3.4 Comparison of equilibrium cores of Westinghouse, CE and MASLWR

Figure 3.12 shows the comparison of antineutrino rate per fission for the equilibrium cores of all the three models that are considered. The Westinghouse (Sequoyah) and CE (SONGS) cores exhibit very similar trends with minor differences. This similarity is most likely because both models had one third of the core loaded with fresh LEU fuel and both operate at similar power densities (110 kW/liter and 106 kW/liter, respectively, for Westinghouse and CE). The MASLWR core emits 1.5%

more antineutrinos per fission than the other core types due to the fact that half of the MASLWR equilibrium core was loaded with fresh LEU assemblies. It was also observed that the change in antineutrino emission rate between the start of the cycle and 340 days (EOC for MASLWR core) into the cycle are 4.3%, 4.2% and 3.3%, respectively, for Westinghouse, CE and MASLWR cores. The change in antineutrino rate per fission is smaller for the MASLWR because of its lower power density (85kW/liter) when compared to the other cores (110kW/liter).

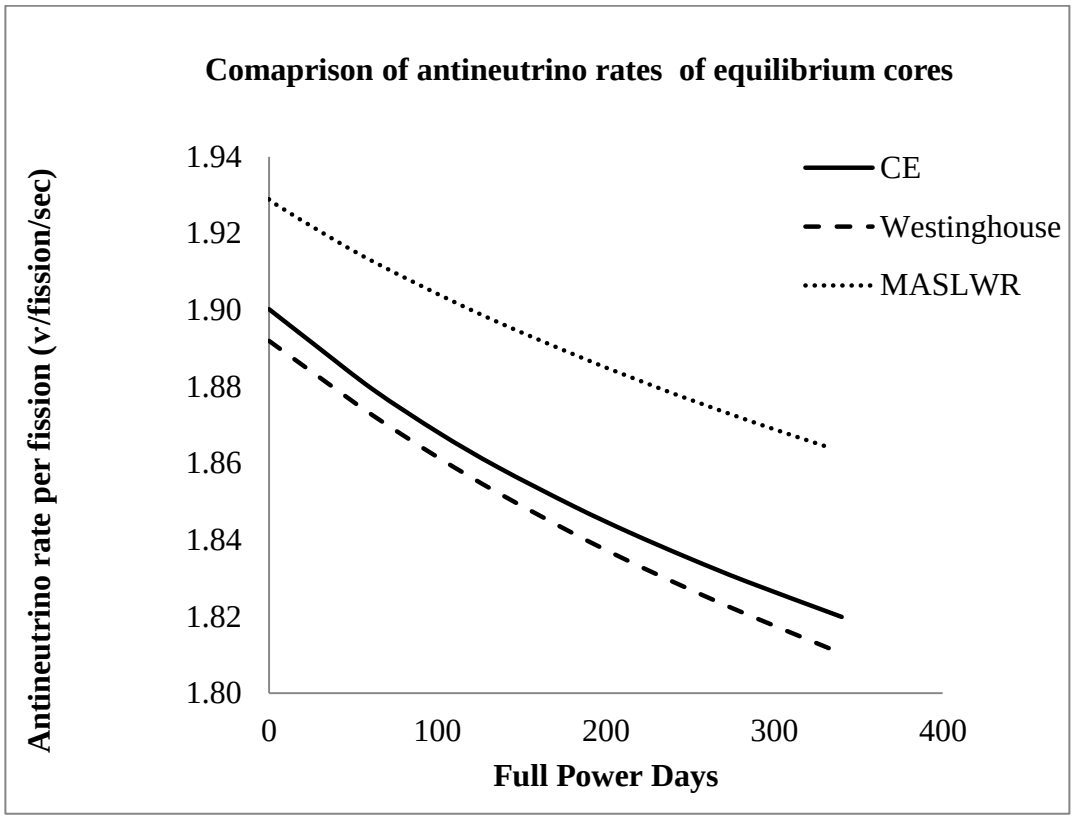

Figure 3.12: Comparison of equilibrium cores of CE, Westinghouse and MASLWR cores

4 Conclusions and Future Work

4.1 Analysis of Results

The fission rates calculated for the SONGS unit 2, cycle 13 from the three-dimensional core simulation using SIMULATE-3 were within ±2.5% of the rough estimate of fission rates. This discrepancy could be attributed to the differences in fission energy of the individual isotopes and energy loss due to radiation. The individual fission rates of isotopes showed trends similar to those predicted in previous simulations. The detector response calculated at an effective detector efficiency of 6.75% from the simulation results is within ±4% of the measured values from the SONGS 1 detector. As a result, the method employed in calculating the fission rates, antineutrino source terms and the detector response from SIMULATE-3 and CASMO-4 simulation is valid for the prediction of the antineutrino signature of LWRs. With this approach, it is possible to predict the antineutrino signatures of cores for which the individual fuel assembly power histories are not known.

The antineutrino source terms of the equilibrium MASLWR core with LEU fuel when compared to cores loaded partially with MOX (half once burnt LEU and half fresh MOX assemblies) are different by a maximum of about 4% at BOC. However, the ability to detect this change will depend on the detector location and efficiency. It was also observed that the difference in antineutrino rates between cores with RG and WG MOX fuel is very minimal and therefore it might not be possible to identify the type of MOX fuel that is loaded in the core using an antineutrino detector.

The removal of 8kg of plutonium from the MASLWR equilibrium core at the middle of the cycle and replacement with fresh assemblies resulted in a spike in the antineutrino rate and the detector response, as expected. The improvement in accuracy of the total detector response calculated from the sum of individual detector responses of each three dimensional node in the core was studied. The difference in counts for a uniformly loaded symmetrical core calculated by the two methods is negligible. However, in cores with asymmetric loading patterns, the point source method yields the same count rate regardless of the location of the assemblies that are replaced, while the count rates calculated from the three-dimensional nodal method show a dependence on the location of the replaced assemblies. This was illustrated for MASLWR by considering the diversion scenario in which seven once burnt fuel assemblies are removed from the core to account for an 8 kg plutonium diversion.

The antineutrino production rate of a Westinghouse core with all fresh fuel during its first cycle is simulated using the data from the Sequoyah reactor's FSAR. It was observed that the change in antineutrino rate of a fresh core is almost twice the change that was observed for an equivalent equilibrium core during the same period. The Westinghouse core was also partially loaded with MOX fuel (one-third MOX) and the predicted antineutrino rate observed is about 2.2% less than that of the equilibrium LEU core and the change would not be distinguishable using a SONGS1 detector because of the error in counting statistics and uncertainty in calculating the antineutrino spectrum.

The comparison of the equilibrium cycles of the three models showed that the antineutrino rate would depend on the percentage of fresh fuel that is loaded in the core and the power density at which the reactor is operated. For cores that operate at lower power densities, the integration time of the detector must be longer to measure changes in the antineutrino rate when compared with cores operating at higher power densities.

4.2 Future work

The total fission rates obtained for the Westinghouse cores with MOX assemblies and LEU assemblies with IFBA burnable poisons were higher by 10% larger than the expected fission rates. This discrepancy is most likely due to some error introduced by the approximate cross-sections calculated from CASMO-4. It would be useful to perform a two-dimensional simulation of the same model using CASMO-4e which has the provisions to model a quarter-core and would give fission rates for the individual isotopes directly.

The simulations can be extended to boiling water reactors (BWRs) as the fission rates of BWRs have significant axial and radial variation and therefore it would be interesting to calculate the detector response using the three dimensional nodal method as it might be possible to observe significant changes in counts with respect to the detector location.

Other improvements that could be made to the model are: inclusion of the shutdown cooling times of assemblies during reshuffling cases to account for xenon and samarium, depletion of the model from zero power to full power gradually in steps

to simulate more realistic operating conditions and other core transient conditions such as control rod insertions and their effect on detector response.

References

Avignone III, F., & Greenwood, Z. “Calculated spectra of antineutrinos from the fission products of ^{235}U, ^{238}U and ^{239}Pu and antineutrino-induced reactions." *Physical Review C*, *22*(2), 594. APS (1980).

Bernstein, A., Wang, Y., Gratta, G., & West, T. “Nuclear reactor safeguards and monitoring with antineutrino detectors.” *Journal of Applied Physics*, *91*(7), 4672. doi:10.1063/1.1452775 (2002).

Bowden, N. S. “Reactor monitoring and safeguards using antineutrino detectors.” *Journal of Physics: Conference Series*, *136*(2), 022008. doi:10.1088/1742-6596/136/2/022008 (2008).

Bowden, N. S., Bernstein, A., Dazeley, S., Svoboda, R., Misner, A, & Palmer, T. “Observation of the Isotopic Evolution of Pressurized Water Reactor Fuel Using an Antineutrino Detector.” *Journal of Applied Physics*, *105*(6), 9 (2008).

Christian, D. A., & Allen, G. “Safety Evaluation By the Office of Nuclear Reactor Regulation Relating to Topical Report Dom-Naf-1 Qualification of the Studsvik Core Management System Reactor Physics Methods for Application to North Anna And Surry Power Stations, Units 1 And 2 Docket No.” *North*. Division of Licensing Project Management, Office of Nuclear Reactor Regulation (2003).

Cribier, M. “Reactor Monitoring with Neutrinos.” *Arxiv preprint arXiv:0704.0891*, (Neutrino), 6-11 (2007).

Dean, D. W. “SIMULATE-3 MOX Enhancements and Verification Tests.” *Studsvik Report, Studsvik of America, USA, SSP-09/441* (2009).

Edenius, M., Ekberg, K., Forssén, B. H., & Knott, D. “CASMO-4, A Fuel Assembly Burnup Program, User’s Manual.” *Studsvik0SOA-9501, Studsvik of America, Inc* (1995).

Gehin, J., Carbajo, J., & Ellis, R. “Issues in the Use of Weapons-Grade MOX Fuel in VVER-1000 Nuclear Reactors: Comparison of UO2 and MOX Fuels.” *ORNL/TM-2004/223, Oak Ridge National Laboratory*. Oak Ridge, Tennessee (2004).

Huber, P., & Schwetz, T. “Precision spectroscopy with reactor anti-neutrinos.” doi:10.1103/PhysRevD.70.053011 (2004).

Duderstadt, J., And L. Hamilton. *Nuclear Reactor Analysis*. John Wiley & Sons, Inc. 1976.

Kozlowski, T., & Downar, T. J. "Pressurised Water Reactor MOX/UO2 Core Transient Benchmark Final Report." *Nuclear Energy Agency* NEA No. 6048 (2006).

MG Sowerby. "Nuclear Fission and Fusion, and neutron interactions." http://www.kayelaby.npl.co.uk/atomic_and_nuclear_physics/4_7/4_7_1.html

Misner, Alex. "Simulated Antineutrino Signatures of Nuclear Reactors for Nonproliferation Applications." *Ph.D Thesis*. Oregon State University (2008).

Nieto, M. M., Hayes, A. C., Teeter, C. M., Wilson, W. B., & Stanbro, W. D. "Detection of Antineutrinos for Non-Proliferation." *International Security*, 1-15 (2003).

SCE, & SDG&E. *Final Safety Analysis Report: San Onofre Nuclear Generating Station Units 2 & 3* (1978).

S.P Palmtag. "Advanced Nodal Methods for MOX Fuel Analysis." *Ph.D Thesis*, Massachusetts Institute of Technology (1997).

Soldatov, A., & Palmer, T. "Design And Analysis Of A Nuclear R Eactor Core For Innovative Small Light Water Reactors." *Ph.D* Thesis, Oregon State University (2009).

TVA. *Sequoyah Nuclear Plant Final Safety Analysis Report Update* (1983).

Umbarger, J. A., & DiGiovine, A. "SIMULATE-3, Advanced Three-Dimensional Two-Group Reactor Analysis Code, User's Manual." *Studsvik Report, Studsvik of America, USA, 103*(4) (1992).

Vogel, P., & Beacom, J. F. "Angular distribution of neutron inverse beta decay." *Physical Review*, *60*, 1-10 (1999).

Report on "Small Nuclear Power Reactors." *World Nuclear Association*. (2011).

Appendices

Appendix A – Core Parameters used in Simulation

Table A- 1: Core parameters used in simulation for the three reactor models

Parameter	CE (SONGS)	MASLWR	Westinghouse (Sequoyah)
Power (MWt)	3640	150	3565
Power Density (kW/liter)	106.3	85	110.07
Total Number of Assemblies	217	24	193
Coolant Flow (Kg/cm^2-hr)	1284	137.6	1201
Assembly Length (cm)	365.76	160	365.76
Assembly type	Westinghouse 16x16	Westinghouse 17x17	Westinghouse 17x17
Assembly Pitch (cm)	20.7	21	21.42
Pressure (Psia)	2250	1247	2250
Fuel Axial Nodes	12	12	12
Reflector Material	Stainless Steel/Water	Stainless Steel/Water	Stainless Steel/Water
Coolant Temperature Inlet (F)	560	420.5	560

Table A- 2: Burnable poison type and boron loading used in Westinghouse Models

Assembly Type	Enrichment	BP type	Density (g/cm^3)	Boron Loading
Fresh LEU assmblies used in Cycle 1 (Case 1)	2.1, 2.6 & 3.1 wt % ^{235}U	Borosilicate Glass	2.23	12.5 wt% B2O3
LEU assemblies in MOX and Equilibrium core(Case 2,3 and 4)	4.2 & 4.0 wt % ^{235}U	IFBA	1.69	100 wt% ZrB2
MOX assemblies	4.3 & 4 wt % Fissile Pu	WABA	3.5635	10 wt % B4C

Appendix B – Table of Fission rates and Antineutrino Source Terms

Table B- 1: Fission rates and antineutrino source terms for SONGS benchmark

Days	^{235}U Fissions	^{238}U Fissions	^{239}Pu Fissions	^{241}Pu Fissions	Total Fissions	Total Antineutrinos
0	8.39E+19	8.21E+18	1.92E+19	4.20E+18	1.15E+20	2.19E+20
27	8.10E+19	8.24E+18	2.14E+19	4.34E+18	1.15E+20	2.18E+20
62	7.77E+19	8.26E+18	2.42E+19	4.61E+18	1.15E+20	2.16E+20
101	7.45E+19	8.27E+18	2.69E+19	4.95E+18	1.15E+20	2.14E+20
136	7.18E+19	8.28E+18	2.90E+19	5.32E+18	1.14E+20	2.13E+20
181	6.88E+19	8.29E+18	3.13E+19	5.84E+18	1.14E+20	2.11E+20
214	6.67E+19	8.30E+18	3.29E+19	6.25E+18	1.14E+20	2.10E+20
249	6.45E+19	8.31E+18	3.44E+19	6.73E+18	1.14E+20	2.09E+20
284	6.25E+19	8.32E+18	3.57E+19	7.21E+18	1.14E+20	2.08E+20
340	5.95E+19	8.33E+18	3.77E+19	8.01E+18	1.14E+20	2.07E+20
375	5.77E+19	8.33E+18	3.89E+19	8.54E+18	1.13E+20	2.06E+20
410	5.59E+19	8.34E+18	4.00E+19	9.06E+18	1.13E+20	2.05E+20
445	5.42E+19	8.34E+18	4.10E+19	9.59E+18	1.13E+20	2.04E+20
473	5.29E+19	8.34E+18	4.18E+19	1.00E+19	1.13E+20	2.04E+20
508	5.13E+19	8.35E+18	4.28E+19	1.05E+19	1.13E+20	2.03E+20
543	4.97E+19	8.35E+18	4.37E+19	1.11E+19	1.13E+20	2.02E+20
571	4.84E+19	8.35E+18	4.44E+19	1.15E+19	1.13E+20	2.02E+20
597	4.73E+19	8.35E+18	4.51E+19	1.19E+19	1.13E+20	2.01E+20
650	4.50E+19	8.36E+18	4.64E+19	1.27E+19	1.12E+20	2.00E+20

Table B- 2: Fission rates and antineutrino source terms for MASLWR case 1

Days	^{235}U Fissions	^{238}U Fissions	^{239}Pu Fissions	^{241}Pu Fissions	Total Fissions	Total Antineutrinos
0	3.88E+18	3.09E+17	4.90E+17	2.72E+16	4.70E+18	9.07E+18
13	3.82E+18	3.10E+17	5.27E+17	3.11E+16	4.69E+18	9.03E+18
25	3.78E+18	3.10E+17	5.59E+17	3.41E+16	4.69E+18	9.01E+18
38	3.75E+18	3.10E+17	5.91E+17	3.74E+16	4.69E+18	8.99E+18
50	3.71E+18	3.10E+17	6.21E+17	4.14E+16	4.69E+18	8.98E+18
63	3.68E+18	3.11E+17	6.50E+17	4.47E+16	4.68E+18	8.96E+18
83	3.62E+18	3.11E+17	6.95E+17	5.10E+16	4.68E+18	8.93E+18
104	3.57E+18	3.11E+17	7.38E+17	5.81E+16	4.68E+18	8.90E+18
125	3.52E+18	3.11E+17	7.80E+17	6.51E+16	4.68E+18	8.88E+18
146	3.47E+18	3.11E+17	8.19E+17	7.23E+16	4.67E+18	8.86E+18
167	3.42E+18	3.11E+17	8.55E+17	7.91E+16	4.67E+18	8.83E+18
188	3.38E+18	3.11E+17	8.91E+17	8.71E+16	4.67E+18	8.81E+18
208	3.34E+18	3.11E+17	9.26E+17	9.41E+16	4.67E+18	8.79E+18
229	3.29E+18	3.11E+17	9.59E+17	1.02E+17	4.66E+18	8.77E+18
250	3.25E+18	3.11E+17	9.91E+17	1.09E+17	4.66E+18	8.75E+18

271	3.21E+18	3.11E+17	1.02E+18	1.18E+17	4.66E+18	8.73E+18
292	3.17E+18	3.11E+17	1.05E+18	1.26E+17	4.66E+18	8.71E+18
313	3.13E+18	3.11E+17	1.08E+18	1.34E+17	4.66E+18	8.69E+18
333	3.09E+18	3.11E+17	1.11E+18	1.41E+17	4.65E+18	8.67E+18
354	3.06E+18	3.11E+17	1.13E+18	1.51E+17	4.65E+18	8.66E+18
375	3.02E+18	3.11E+17	1.16E+18	1.59E+17	4.65E+18	8.64E+18
417	2.95E+18	3.11E+17	1.21E+18	1.77E+17	4.65E+18	8.62E+18
458	2.95E+18	3.08E+17	1.21E+18	1.77E+17	4.64E+18	8.60E+18

Table B- 3: Fission rates and antineutrino source terms for MASLWR case 2

Days	^{235}U Fissions	^{238}U Fissions	^{239}Pu Fissions	^{241}Pu Fissions	Total Fissions	Total Antineutrinos
0	2.33E+18	3.24E+17	1.69E+18	2.75E+17	4.62E+18	8.33E+18
13	2.33E+18	3.25E+17	1.68E+18	2.74E+17	4.61E+18	8.32E+18
25	2.31E+18	3.25E+17	1.70E+18	2.80E+17	4.61E+18	8.31E+18
38	2.28E+18	3.25E+17	1.73E+18	2.85E+17	4.61E+18	8.30E+18
50	2.25E+18	3.25E+17	1.75E+18	2.91E+17	4.61E+18	8.29E+18
63	2.23E+18	3.25E+17	1.77E+18	2.97E+17	4.62E+18	8.28E+18
83	2.19E+18	3.25E+17	1.80E+18	3.07E+17	4.62E+18	8.27E+18
104	2.14E+18	3.25E+17	1.83E+18	3.17E+17	4.61E+18	8.25E+18
125	2.11E+18	3.25E+17	1.86E+18	3.29E+17	4.62E+18	8.24E+18
146	2.07E+18	3.25E+17	1.88E+18	3.40E+17	4.62E+18	8.22E+18
167	2.03E+18	3.25E+17	1.91E+18	3.51E+17	4.62E+18	8.21E+18
188	1.99E+18	3.25E+17	1.94E+18	3.64E+17	4.62E+18	8.20E+18
208	1.96E+18	3.25E+17	1.96E+18	3.74E+17	4.62E+18	8.19E+18
229	1.92E+18	3.25E+17	1.98E+18	3.87E+17	4.62E+18	8.18E+18
250	1.89E+18	3.25E+17	2.01E+18	3.98E+17	4.62E+18	8.16E+18
271	1.85E+18	3.25E+17	2.03E+18	4.10E+17	4.62E+18	8.15E+18
292	1.82E+18	3.25E+17	2.05E+18	4.22E+17	4.62E+18	8.14E+18
313	1.79E+18	3.25E+17	2.07E+18	4.34E+17	4.62E+18	8.13E+18
333	1.76E+18	3.25E+17	2.09E+18	4.46E+17	4.62E+18	8.12E+18
354	1.76E+18	3.23E+17	2.09E+18	4.46E+17	4.62E+18	8.12E+18

Table B- 4: Fission rates and antineutrino source terms for MASLWR case 3

Days	^{235}U Fissions	^{238}U Fissions	^{239}Pu Fissions	^{241}Pu Fissions	Total Fission	Total Antineutrinos
0	2.14E+18	3.22E+17	2.10E+18	5.34E+16	4.61E+18	8.14E+18
13	2.16E+18	3.23E+17	2.08E+18	5.80E+16	4.61E+18	8.15E+18
25	2.14E+18	3.23E+17	2.09E+18	6.32E+16	4.61E+18	8.14E+18
38	2.12E+18	3.23E+17	2.10E+18	6.74E+16	4.61E+18	8.14E+18
50	2.10E+18	3.23E+17	2.12E+18	7.33E+16	4.61E+18	8.13E+18
63	2.08E+18	3.23E+17	2.13E+18	7.87E+16	4.61E+18	8.13E+18
83	2.05E+18	3.23E+17	2.15E+18	8.81E+16	4.61E+18	8.11E+18
104	2.02E+18	3.23E+17	2.18E+18	9.83E+16	4.62E+18	8.11E+18
125	1.98E+18	3.23E+17	2.20E+18	1.08E+17	4.62E+18	8.10E+18
146	1.95E+18	3.23E+17	2.22E+18	1.19E+17	4.62E+18	8.09E+18
167	1.92E+18	3.23E+17	2.24E+18	1.28E+17	4.62E+18	8.08E+18
188	1.89E+18	3.23E+17	2.27E+18	1.38E+17	4.62E+18	8.07E+18
208	1.86E+18	3.23E+17	2.28E+18	1.49E+17	4.62E+18	8.06E+18
229	1.83E+18	3.23E+17	2.30E+18	1.60E+17	4.62E+18	8.05E+18
250	1.81E+18	3.23E+17	2.32E+18	1.71E+17	4.62E+18	8.04E+18
271	1.78E+18	3.23E+17	2.34E+18	1.81E+17	4.62E+18	8.03E+18
292	1.75E+18	3.23E+17	2.36E+18	1.93E+17	4.62E+18	8.03E+18
313	1.72E+18	3.23E+17	2.37E+18	2.04E+17	4.62E+18	8.02E+18
333	1.69E+18	3.23E+17	2.39E+18	2.16E+17	4.62E+18	8.01E+18
354	1.67E+18	3.23E+17	2.41E+18	2.27E+17	4.63E+18	8.00E+18
375	1.64E+18	3.23E+17	2.42E+18	2.38E+17	4.63E+18	8.00E+18
417	1.59E+18	3.23E+17	2.46E+18	2.62E+17	4.63E+18	7.99E+18
458	1.59E+18	3.22E+17	2.45E+18	2.63E+17	4.63E+18	7.98E+18

Table B- 5: Fission rates and antineutrino source terms for MASLWR case 4

Days	^{235}U Fissions	^{238}U Fissions	^{239}Pu Fissions	^{241}Pu Fissions	Total Fissions	Total Antineutrinos
0	9.42E+17	3.53E+17	2.69E+18	5.46E+17	4.53E+18	7.67E+18
13	1.02E+18	3.49E+17	2.63E+18	5.36E+17	4.53E+18	7.70E+18
25	1.03E+18	3.49E+17	2.61E+18	5.42E+17	4.53E+18	7.71E+18
38	1.04E+18	3.48E+17	2.60E+18	5.46E+17	4.53E+18	7.72E+18
50	1.04E+18	3.47E+17	2.59E+18	5.52E+17	4.54E+18	7.73E+18
63	1.05E+18	3.47E+17	2.58E+18	5.58E+17	4.54E+18	7.74E+18
83	1.06E+18	3.46E+17	2.57E+18	5.68E+17	4.54E+18	7.75E+18
104	1.07E+18	3.45E+17	2.56E+18	5.77E+17	4.54E+18	7.76E+18
125	1.07E+18	3.44E+17	2.54E+18	5.87E+17	4.55E+18	7.77E+18
146	1.08E+18	3.43E+17	2.53E+18	5.97E+17	4.55E+18	7.78E+18

167	1.08E+18	3.42E+17	2.52E+18	6.06E+17	4.55E+18	7.79E+18
188	1.09E+18	3.42E+17	2.51E+18	6.15E+17	4.56E+18	7.80E+18
208	1.09E+18	3.41E+17	2.50E+18	6.25E+17	4.56E+18	7.80E+18
229	1.10E+18	3.40E+17	2.49E+18	6.34E+17	4.56E+18	7.81E+18
250	1.10E+18	3.39E+17	2.48E+18	6.43E+17	4.56E+18	7.82E+18
271	1.10E+18	3.39E+17	2.47E+18	6.53E+17	4.57E+18	7.83E+18
292	1.11E+18	3.38E+17	2.46E+18	6.62E+17	4.57E+18	7.83E+18
313	1.11E+18	3.37E+17	2.45E+18	6.70E+17	4.57E+18	7.84E+18
333	1.12E+18	3.36E+17	2.45E+18	6.69E+17	4.57E+18	7.84E+18

Table B- 6: Fission rates and antineutrino source terms for MASLWR case 5

Days	^{235}U Fissions	^{238}U Fissions	^{239}Pu Fissions	^{241}Pu Fissions	Total Fissions	Total Antineutrinos
0	9.71E+17	3.07E+17	3.19E+18	5.95E+16	4.53E+18	7.46E+18
13	1.02E+18	3.11E+17	3.14E+18	6.61E+16	4.54E+18	7.50E+18
25	1.03E+18	3.12E+17	3.12E+18	7.38E+16	4.54E+18	7.51E+18
38	1.03E+18	3.13E+17	3.11E+18	8.12E+16	4.54E+18	7.52E+18
50	1.04E+18	3.14E+17	3.10E+18	8.90E+16	4.54E+18	7.53E+18
63	1.04E+18	3.15E+17	3.10E+18	9.70E+16	4.55E+18	7.54E+18
83	1.04E+18	3.16E+17	3.08E+18	1.10E+17	4.55E+18	7.55E+18
104	1.04E+18	3.18E+17	3.07E+18	1.24E+17	4.55E+18	7.56E+18
125	1.05E+18	3.19E+17	3.06E+18	1.38E+17	4.56E+18	7.57E+18
146	1.05E+18	3.20E+17	3.04E+18	1.51E+17	4.56E+18	7.58E+18
167	1.05E+18	3.21E+17	3.03E+18	1.66E+17	4.56E+18	7.59E+18
188	1.04E+18	3.22E+17	3.02E+18	1.81E+17	4.56E+18	7.60E+18
208	1.04E+18	3.23E+17	3.00E+18	1.96E+17	4.57E+18	7.61E+18
229	1.04E+18	3.24E+17	2.99E+18	2.11E+17	4.57E+18	7.62E+18
250	1.04E+18	3.25E+17	2.98E+18	2.26E+17	4.57E+18	7.63E+18
271	1.04E+18	3.27E+17	2.97E+18	2.42E+17	4.57E+18	7.64E+18
292	1.04E+18	3.28E+17	2.95E+18	2.58E+17	4.58E+18	7.65E+18
313	1.03E+18	3.29E+17	2.94E+18	2.74E+17	4.58E+18	7.66E+18
333	1.03E+18	3.30E+17	2.93E+18	2.89E+17	4.58E+18	7.67E+18
354	1.03E+18	3.31E+17	2.92E+18	3.06E+17	4.58E+18	7.68E+18
375	1.03E+18	3.32E+17	2.90E+18	3.21E+17	4.58E+18	7.69E+18
417	1.02E+18	3.34E+17	2.88E+18	3.54E+17	4.59E+18	7.70E+18
458	1.01E+18	3.36E+17	2.85E+18	3.86E+17	4.59E+18	7.72E+18
500	1.01E+18	3.38E+17	2.83E+18	4.19E+17	4.59E+18	7.73E+18
542	9.99E+17	3.40E+17	2.81E+18	4.51E+17	4.59E+18	7.75E+18
583	9.90E+17	3.42E+17	2.78E+18	4.84E+17	4.60E+18	7.76E+18
625	9.82E+17	3.44E+17	2.76E+18	5.16E+17	4.60E+18	7.78E+18
667	9.73E+17	3.46E+17	2.74E+18	5.48E+17	4.60E+18	7.79E+18

Table B- 7: Fission rates and antineutrino source terms for Sequoyah fresh core (case 1)

Days	^{235}U Fissions	^{238}U Fissions	^{239}Pu Fissions	^{241}Pu Fissions	Total Fissions	Total Antineutrinos
0	1.05E+20	8.10E+18	0	0	1.13E+20	2.24E+20
8	1.02E+20	8.12E+18	1.88E+18	0	1.12E+20	2.22E+20
17	9.95E+19	8.15E+18	4.31E+18	0	1.12E+20	2.20E+20
27	9.64E+19	8.20E+18	7.12E+18	0	1.12E+20	2.18E+20
62	8.76E+19	8.31E+18	1.50E+19	2.50E+17	1.11E+20	2.13E+20
101	7.99E+19	8.39E+18	2.17E+19	7.69E+17	1.11E+20	2.10E+20
136	7.42E+19	8.44E+18	2.65E+19	1.43E+18	1.11E+20	2.07E+20
181	6.80E+19	8.50E+18	3.14E+19	2.47E+18	1.10E+20	2.04E+20
214	6.40E+19	8.53E+18	3.43E+19	3.31E+18	1.10E+20	2.02E+20
249	6.02E+19	8.55E+18	3.69E+19	4.24E+18	1.10E+20	2.00E+20
284	5.67E+19	8.57E+18	3.92E+19	5.20E+18	1.10E+20	1.99E+20
340	5.66E+19	8.53E+18	3.92E+19	5.21E+18	1.10E+20	1.98E+20